AIAA JOURNAL
Vol. 56, No. 3, March 2018

Active Control of Noise from Hot Supersonic Jets

Aniruddha Sinha,* Aaron Towne,† and Tim Colonius‡
California Institute of Technology, Pasadena, California 91106
and
Robert H. Schlinker,§ Ramons Reba,¶ John C. Simonich,** and Daniel W. Shannon††
United Technologies Research Center, East Hartford, Connecticut 06108

DOI: 10.2514/1.J056159

This paper presents diagnostic experiments aimed at understanding and mitigating supersonic jet noise from the coherent wave-packet structures that are the source of peak aft-angle mixing noise. Both isothermal and heated, nearly perfectly expanded, Mach 1.5 jets were forced in the near-nozzle region with air injection generated by a spinning-valve device designed to excite the jet at frequencies approaching those of the dominant turbulent structures. Substantial reductions in the peak aft-angle radiation were achieved with steady blowing at amplitudes corresponding to 2–6% of the mass flow rate of the primary jet. The noise benefit saturated at mass flow rates above 4%, with as much as a 6 dB reduction in overall sound pressure level at aft angles. Increasing the mass flow rates yielded a monotonically increasing high-frequency noise penalty at the sideline, where noise levels in the natural jet were already 15 dB lower than the aft-angle peak, so that the penalty due to actuation was minor. Although both steady and periodic unsteady mass injections were produced by the spinning valve when it rotated, it was calibrated to hold the steady mass flow rate constant as the frequency of unsteady blowing was changed. In this way, the effect of steady and unsteady blowings on the acoustic field could be decoupled. It is shown that the noise benefit was uniquely associated with the steady component of blowing, whereas the unsteady component resulted in additive tones in the spectra. This implied linearity is consistent with theory and experiments showing that the wave-packet structures, which give rise to the dominant aft-angle radiation, evolve in the turbulent mean flowfield in a nearly linear fashion from their origin in the near-nozzle region. The interpretation of noise reduction is that the steady component of blowing spreads the mean flow more rapidly, resulting in weaker wave packets. Periodic unsteady blowing forces coherent wave packets that are largely uncorrelated from the random natural ones, which then leads to the observed additive tones.

I. Introduction

HIGH noise levels associated with the supersonic jet exhaust of current and future tactical military aircraft pose health problems for aircraft carrier launch/recovery crews and community noise issues. Reduction of supersonic jet noise thus poses a significant research challenge for future aircraft. Current programs directed at supersonic military engine noise reduction are demonstrating benefits of several decibels using passive and active methods to increase jet mixing and break up shock cells (in case of overexpanded jets). These achieve modest noise reduction but with adverse impact on aircraft weight, performance, and survivability. New approaches are needed to address supersonic exhaust noise reduction.

In this paper, we present results from the application of a spinning-valve actuator for steady or pulsed air injection close to the nozzle lip with the purpose of supersonic jet noise mitigation. This spinning valve was developed at United Technologies Research Center (UTRC) [1], and its use was previously demonstrated in active control of combustion instabilities [2,3]. Extensive diagnostics deployed in the present experiments allowed a detailed analysis of the mechanism of jet noise reduction.

A. Sources of Supersonic Jet Noise

High levels of turbulence associated with the jet flow are related to large-scale turbulent structures that advect and evolve in the jet plume, as well as finer-scale turbulence that results from secondary instabilities and the turbulence cascade. When the coherent structures have supersonic convection velocities, they are capable of directly radiating to the far field by analogy with supersonic flow over a wavy wall [4]. Because their advection velocity is some fraction (typically 0.6 to 0.7) of the jet Mach number, they do not radiate directly until the jet Mach number is well into the supersonic range. However, even at subsonic speeds, coherent structures radiate sound due to their growth, saturation, and decay [5]. Through their nonlinear interaction over a range of turbulent scales, these structures extract energy from the flow and are primarily responsible for the observed spreading of the mean jet plume. The sound radiated by these large-scale structures dictates the aft directivity peak and represents the most energetic component of the turbulent mixing noise. Although attenuation of jet mixing noise is the concern of this paper, we note for completeness that there are two other sources of noise (viz., broadband shock-associated noise and screech) that are important in nonideally expanded supersonic jets.

B. Previous Efforts at Active Control of Jet Noise

Currently, passive methods to increase jet mixing and break up shock cells in the overexpanded flow are being considered to reduce noise levels. These include nozzle serrations (chevrons) [6,7] and lobed nozzle inserts to achieve ideal expansion [8]. These passive methods have achieved noise reductions of up to a few decibels.

Active, deployable approaches that could avoid performance penalties in mission-critical portions of the flight envelope are a desirable alternative. A review was recently published on the proven active approach of water and air injection at the nozzle lip [9]. At the time of that review, water injection was found to produce the largest

Received 15 March 2017; revision received 13 October 2017; accepted for publication 15 October 2017; published online 23 November 2017.

*Currently Assistant Professor, Aerospace Engineering, Indian Institute of Technology Bombay, Mumbai 400 076, India.
†Currently Postdoctoral Fellow, Center for Turbulence Research, Stanford University, Stanford, California 94305.
‡Professor, Mechanical Engineering.
§Currently retired, 21382 Amora, Mission Viejo, California 92692.
¶Program Element Leader, Compression Technologies.
**Currently retired, P.O. Box 1407, Mendocino, California 95460.
††Senior Research Scientist.

reduction in peak jet mixing noise, with up to 6 dB in overall sound pressure level (OASPL), but requiring 17% of the jet mass flow rate in injected water [10]. In these earlier studies, steady air injection produced smaller noise reductions, but work concurrent to the present study has reported about a 2.2 dB OASPL reduction at a 3% mass flow rate [11]. In steady blowing, streamwise vortices generated near the nozzle enhance the mixing in a manner similar to chevrons [12]. In addition to reduction of the jet mixing noise, steady fluidic injection inside the diverging section of the nozzle can be used to reduce shock-associated noise in imperfectly expanded jets [13].

Unsteady actuation strategies have also been recently investigated. One study using pulsed fluidic injection reported that improvements in the noise benefit to mass input ratio may be achievable through optimized unsteady injection [14]. Significant noise reductions have also been achieved with pulsating plasma actuation at the nozzle lip [15]. The mechanisms by which noise reduction is achieved by these unsteady actuation approaches, however, have not been fully explained.

On the contrary, a thorough investigation of the control mechanism was recently reported for an actuation system consisting of steady fluidic injection but from a rotating centerbody in the jet [16]. Using detailed diagnostic measurements, the authors were able to link the observed noise reduction to the weakened wave-packet dynamics in the deformed turbulent mean flowfield. The latter change was due to the generation of incoherent Reynolds stresses by actuation at a frequency–azimuthal mode combination to which the mean flow was stable. On the other hand, noise amplification was reported with actuation in an unstable mode, with the response dominated by coherent structures amplified beyond the linear limit.

A study with a similar intent to reduce noise, albeit in a low-Reynolds-number planar mixing layer, using feedforward control was recently reported [17]. Using the linear instability wave-packet approach, the authors were able to derive a control law based on phase opposition whose application in numerical simulation resulted in attenuation of unsteady fluctuations in the mixing layer. This approach holds promise for real-time flow control of wave-packet-generated noise with phase opposition to the nascent random fluctuations.

C. Linear Wave-Packet Model of Noise

Wave packets are coherent large-scale advecting structures in the turbulent flow that dominate the pressure field just outside the jet shear layer. These have been observed since the early years of jet noise research [18], and they have been the subject of continuing investigations [5,19–23]. These structures can be observed over a range of frequencies and with varying azimuthal structure, but they are typically dominated by the first few azimuthal modes (i.e., axisymmetric, first helical mode, etc.). For many years, researchers have sought to model these observed structures in terms of instability waves [24–29] of both transitional and fully turbulent jets. In the context of free shear flows, instability waves represent convecting disturbances that grow in space and/or time and are solutions of an eigenvalue problem (modes) associated with infinitesimal (linear) disturbances to a time-invariant transversely sheared flow. An important aspect of wave packets is that, when their phase speed is supersonic with respect to the ambient sound speed, they directly radiate Mach waves [28], and are therefore an appropriate target for active noise control.

For natural (unforced) jets, large-scale structures occur stochastically and are difficult to distinguish precisely from the background turbulence spanning a range of scales. However, using an extensive caged microphone array placed in the near-jet pressure field, the distinct characteristics of instability waves associated with the experimentally determined mean velocity field were conclusively identified in natural turbulent (cold and hot) jets at high subsonic speeds at NASA John H. Glenn Research Center (GRC) [22]. Just outside the jet shear layer, where disturbances from less coherent smaller-scale motions have decayed sufficiently, the instability waves induce exponentially decaying, evanescent (for subsonic convection speed) pressure waves. This pressure field accounts for the dominant part of the microphone signal and is, in fact, synonymous with the previously mentioned wave packets in the near-pressure field.

Reba et al. [23] investigated the extent to which the far acoustic field could be directly predicted based solely on the stochastic amplitude and phase speeds of wave packets measured along the hydrodynamic microphone array using a Kirchhoff surface approach. Good agreement was obtained between the projected stochastic near-field wave packets and far-field sound measured directly on another caged array [30], especially for those operating conditions where the wave-packet evolution was well resolved by the limited spatial extent of the microphone array. The study confirmed the relevance of the large-scale instability wave/wave-packet structures to the acoustic field at subsonic speeds.

In recent years, encouraging success has been achieved in modeling the wave packets in round jets using linear parabolized stability equations (PSE) [31–33], as validated in extensive comparisons with the NASA GRC hydrodynamic microphone array data, as well as state-of-the-art large-eddy simulation (LES) databases [34]. The PSE model shows promise, even in the more complex case of jets issuing from serrated (chevron) nozzles [35]. In the case of supersonic round jets, a moderately good prediction of the radiated acoustic field has also been demonstrated for the PSE model [33]. However, wave-packet "jitter," as will be discussed in the next section, is also an important issue, especially for subsonic jets.

D. Importance of Wave-Packet Jitter

Although the near field of wave packets computed using linear theory, where the long-time average is used as the base flow, exhibits compelling agreement with experiments, the associated sound field level is somewhat underpredicted. In subsonic and low supersonic jets, this underprediction can become severe. The reason for the discrepancy is the statistical variability (termed jitter) of the wave packets, which results in amplification of the acoustic field beyond what is produced by the average wave packet [36–39]. The amplification mechanism is related to the high sensitivity of the acoustic field to the wave-packet envelope shape: the average far-field intensity depends not only on the average wave packet but also on the strongest ones that can exist intermittently.

Although efforts to model the wave-packet variability have not yet yielded satisfactory predictive models, it has suggested a possible mechanism for jet noise reduction. In previous theoretical work, adjoint-based optimal control theory was applied to direct and large-eddy simulations of low-Reynolds-number turbulent jets [40,41]. The control input was a body force near the nozzle exit that was adjusted to minimize the acoustic radiation to locations in the far field. The optimization was shown to reduce noise by tackling the loudest wave packets, essentially eliminating them by subtly changing their phase to reduce the jitter that leads to their amplification.

These studies proved the potential of decreasing wave-packet jitter to achieve jet noise reduction. However, the requisite body-force actuation was a complex function of space and time, and full-state feedback was used in the optimization. Such techniques have no realistic counterpart in real hardware. We hypothesize here that similar changes to wave-packet regularity could be produced, with realistic actuation, by forcing the jet with a suitably low frequency. Estimates of the timescale of intermittency give $St < 0.1$, which is reasonably well separated from the frequencies of peak wave-packet activity in the jet. By organizing the flow at the lower frequency, one may expect that the dominant wave packets would become more organized because they would now evolve in a phase-locked slowly varying flow rather than the intermittent one that exists naturally.

E. Objectives of Present Research

The present research was aimed at understanding the possible mechanisms of noise attenuation in high-Reynolds-number supersonic jets through active control. To this end, we established an experimental setup whereby we could force the wave packets with unsteady blowing. Additionally, we deployed sufficient experimental diagnostics to discern the effect of the forcing on the natural and forced spectrum of excited wave-packet structures. As discussed previously, a linear mechanism of noise reduction was confirmed with the spinning fluidic injector in a low subsonic round jet [16]. Our linear PSE model also delivered

Table 1 Jet operating conditions

Case	Description	NPR	NTR	M_j	M_∞	T_j	Re_j	M_t
B118	Isothermal nearly perfectly expanded	3.55	1.45	1.5	1.5	1.0	16.2×10^5	0.05
B122	Heated nearly perfectly expanded	3.51	2.53	1.5	1.98	1.74	8.2×10^5	0.05

encouraging agreement with experiments and LES data. Hence, our investigation was particularly focused on determining if noise attenuation in jets with supersonic convection speeds may be explained by a linear mechanism.

II. Experimental Setup

A. United Technologies Research Center Acoustic Research Tunnel

Experimental studies were conducted in the UTRC Acoustic Research Tunnel developed in 1970 as the first forward-flight simulation facility for jet noise, fan and propeller noise, and lifting surface/airframe noise studies. The facility can achieve forward-flight simulations up to a freestream tunnel Mach number M_t of 0.6 using wind-tunnel nozzles of different diameters up to 1.27 m (50 in.). The current test used a 0.91 m (36 in.) diameter nozzle, which limited M_t to less than 0.3. The facility can deliver stagnation temperatures up to 671°C and jet Mach numbers up to 2.5 based on the 2.8 MPa supply air. The air is heated with a liquid-propane burner. The test section is surrounded by a sealed chamber 4.9 m (16 ft) high, 5.5 m (18 ft) long (jet centerline direction), and 6.7 m (22 ft) wide, which is anechoic above 175 Hz.

The acoustic facility characteristics were documented in many early reports since its construction [42,43]. The latter provided free-field decay confirmation as well as details of nozzle exhaust flow variations that, during the course of a jet noise run, varied by ±0.1 EPNL at most.

B. Nozzle and Operating Conditions Considered

A thin-lipped method-of-characteristics converging–diverging nozzle with an exit diameter D of 50.8 mm (2 in.) was designed for a jet exit Mach number M_j of 1.5. Two shock-free (to the extent possible) flow conditions, one isothermal and one heated, were considered; see Table 1. The acoustic Mach number M_∞, the nozzle exit static temperature ratio (referenced to the ambient) T_j, the tunnel (coflow) Mach number M_t, the nozzle pressure ratio (NPR), the nozzle temperature ratio (NTR), and the nozzle exit Reynolds number Re_j are given for both operating conditions. These operating conditions were also tested in experiments at NASA GRC [6]; in fact, the terminology of B118 and B122 come from Tanna's jet database [44].

For a fixed NTR, the NPR was varied over a range of values to minimize noise at the 90 deg (sideline) far-field microphone; the NPR at which the minimum value occurred is the value listed in Table 1. This has the effect of assuring shock-free flow, to the extent possible, for the real flow with finite boundary-layer thickness inside the nozzle [45].

C. Spinning-Valve Actuator and Azimuthal Mode Generation

The actuator used to force the jet is a spinning valve developed at UTRC [1]. Air supply is provided to a plenum inside a rotating drum (which is connected to a motor spool) with 40 holes around the periphery; see schematic in Fig. 1a. Concentric to the rotating drum is an outer stationary cylinder having two diametrically opposed holes connected to injection ports. When the motor is operated at a fixed speed, air is delivered to the two outer (stationary) drum holes in a periodic (in-phase) fashion. An additional hole in the housing is clocked to provide an optional 180-deg-out-of-phase flow. During any particular experiment, either this out-of-phase hole or the in-phase hole was used (the other being plugged) along with the primary (reference) hole. When the motor is not operated but the shaft is fixed at a preset rotation angle, steady flow issues from the exit ports. Air injection using the spinning valve is a useful choice of actuation because it provides significant momentum addition to the jet when compared to synthetic jets or plasma actuation. Unlike conventional reciprocating-spool configurations, the upper frequency limit of the spinning valve is not due to the spool inertia or power required to accelerate it.

The maximum rpm of the spinning valve used in the tests was 5000. The forcing frequency f_F is determined by the rpm and the hole count on the rotating drum. We report this in terms of the forcing Strouhal number of $St_F := f_F D/U_j$, where U_j is the exit velocity of the primary jet. Two such actuators with independent (but synchronizable), computer-controlled servomotors are used to inject air into the shear layer of the jet normal to the primary jet axis in most cases; the assembly is shown in Fig. 1b. As shown in the schematic of Fig. 1c, each spinning valve feeds a pair of diametrically opposed ports through the in-phase or out-of-phase housing holes, so that n in the figure is either zero or one. By suitably phasing the two motors (i.e., selecting ϕ) and choosing the integer n, we can simulate perturbation at different azimuthal Fourier modes μ. The phase between the injection ports (A, B, C, and D) for the μ possible are given in Table 2. The $\mu = \pm 1$ is a flapping mode, with the flapping plane located between ports A and B on one side and ports C and D on the other (see Fig. 1c). Note that we refer to the azimuthal patterns of the actuator by the symbol μ to distinguish them from the actual Fourier azimuthal content of the flowfield m.

The air injection generated by the actuator is a strong function of the geometric parameters of the injection nozzle and the plumbing

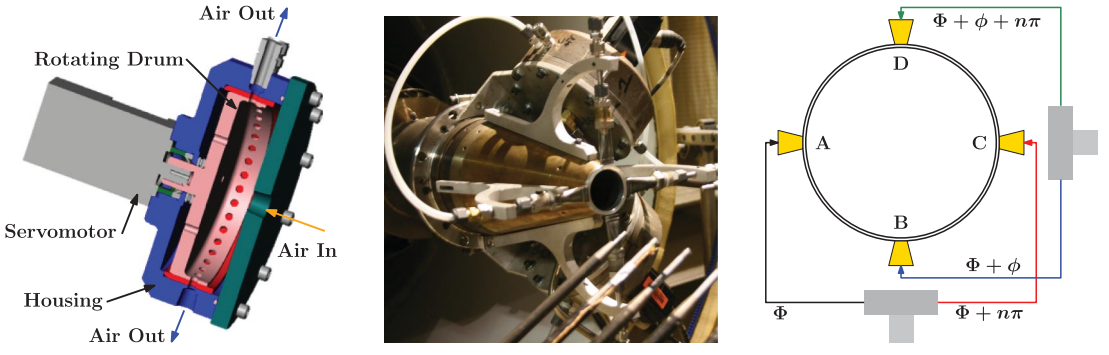

Fig. 1 Representations of a) spinning valve with servomotor, b) two spinning valves installed with injection ports (original design) at 90 deg to the jet flow, and c) phasing of the two motors and the injection ports for different azimuthal forcing patterns.

Table 2 Azimuthal modes of spinning-valve operation (phases in degrees)

	Relative phase at ports					
Actuation pattern, μ	A	B	C	D	Phase between two ports of same valve, $n\pi$	Phase between two motors, ϕ
0	0	0	0	0	0	0
1	0	90	180	270	180	90
±1	0	0	180	180	180	0
±2	0	180	0	180	0	180

from the valve stator to the nozzle, apart from the design of the spinning valve itself. The experiments reported in this paper were performed in two campaigns. In the first one, the actuator system was reused from the original development [1] so that its utility for jet noise mitigation could be established preliminarily. In particular, the injector was essentially a flattened tube with the flat edge aligned parallel to the nozzle trailing edge (see Fig. 1b). Subsequently, the actuation system was completely redesigned to reduce parasitic losses due to flow separations in the injection nozzles and their upstream plumbing. As part of this effort, we specially designed a nozzle (depicted in the inset of Fig. 2) that held the cross-section area constant through a change in shape from the inlet round piping to a thin, elliptical outlet designed to distribute the injected flow over a substantial portion of the jet periphery. The second test campaign used the redesigned actuator system, with identical feed tubing length and identical connections and transitions, providing significantly improved results. Because all the tests in the first campaign were not repeated in the second one, we will show results from both. The two actuator system iterations will be termed "original" and "improved," respectively.

D. Spinning-Valve Characterization

Detailed characterization tests were carried out with the original actuator system, with the results being used to establish the behavior of the spinning valve itself. The characterization tests were partially repeated with the improved actuator system to determine the effect of the design changes. Results from both of these setups will be presented to bring out the behavior of the different components of the actuation system.

The amplitude of actuation is controlled by setting the supply pressure to the spinning valve. The mass flow rate through the spinning valves (measured with a rotameter) increases monotonically with the supply pressure as shown in Fig. 2. In this figure, the actuator mass flow rate is reported as a percentage of the primary jet mass flow rate for the heated jet (case B122). We note that the reduction of flow losses in the improved actuation system boosts the mass flow rate for a given supply pressure measured upstream of the spinning valve.

Hot-wire anemometry was used to record the centerline velocity at the injection port exit of the original actuation system, and it was phase averaged with respect to the actuation pulse. This was facilitated by the simultaneous acquisition of the encoder signals from the servomotors. The air temperature was measured during both hot-wire calibration and measurements, and the hot-wire velocity was corrected for changes in temperature [46]. Mach number effects were accounted for using the known static pressure at the nozzle exit and the measured flow total temperature upstream of the nozzle. The hot wire at these flow rates was essentially measuring density times velocity, and the latter could be found from isentropic relationships. The waveform of the injection velocity is presented in Fig. 3a for the case of 667 pulses/s (i.e., the motor was spinning at 1000 rpm, and it will be recalled that the rotor had 40 holes). This translates to a forcing Strouhal number of $St_F = 0.05$ when referred to the exit velocity and diameter of the heated primary jet. Owing to latencies in the piping downstream of the valve, the waveform departs from a rectangular shape.

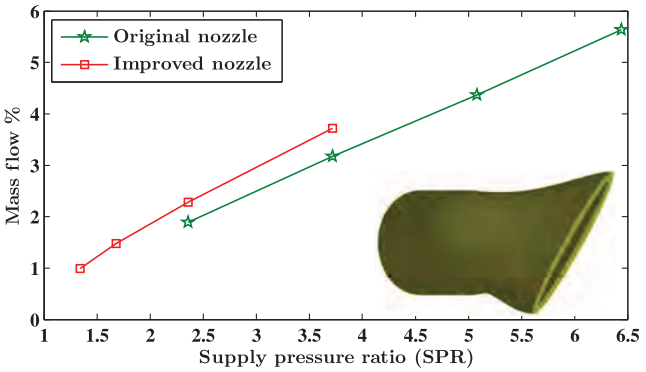

Fig. 2 Total mass flow rate through the two spinning valves (as a percentage of the primary mass flow rate of the heated jet) versus the supply pressure (as a ratio of the atmospheric), for the original and improved injection nozzles. The inset shows a model of the latter.

The steady component of excitation is seen to be a monotonic function of only the mass flow rate in Fig. 3b, irrespective of the rotation rate of the valves, including steady blowing. The pulsatile component of excitation is characterized by the standard deviation of the phase-averaged signature. Figure 3c demonstrates that the pulsatile component depends on the rotation rate of the valves, but it is only a weak function of the mass flow rate. However, the pulsatile content decreases monotonically with increasing pulse frequency, as shown in Fig. 3d. These trends have been noticed in similar actuation systems in [47], where a lumped-element model was proposed to explain the observations.

In the original actuation system as documented previously, the pulsatile component of blowing is modest as compared to the steady offset (mean value). The improved design of the injector nozzle and upstream piping avoided much of the parasitic flow losses. Such losses not only reduce the achievable mass flow rate (see Fig. 2) but they also attenuate the unsteady component of the injection, relative to its steady offset. Figure 3d shows results from the hot-wire survey, with the new design more than doubling the unsteady component of velocity measured near the center of the injector jet over the full range of forcing frequencies. A detailed calibration of the unsteady velocity at the nozzle exit was made to map the injection pressure to the mass flow rate across the range of drum rotation rates. This permits us to hold either the mean or fluctuating component of injection fixed as we vary the frequency. Our subsequent results will demonstrate that holding the mean mass flow rate constant across both steady and unsteady actuations provides a useful basis on which to gauge their relative effectiveness.

E. Microphone Arrays

Motivated by our results linking instability waves/wave packets and peak noise radiation in simple round jets, a wave-packet-based diagnostic technique was further developed to address nonaxisymmetric jet flows of technological relevance, including chevron nozzles and jets forced at higher azimuthal modes [48]. The novel hydrodynamic near-field rotating array concept employs two linear arrays: one fixed, and the second free to rotate azimuthally (see Figs. 4a and 4b). This enables cross correlations to be measured as a function of azimuthal separation and, through appropriate signal processing (see Appendix A), effectively reproduces the effect of a conventional fixed array but with dramatically lower microphone count. In the present experiments, each linear array consists of 16 B&K-type 4939 quarter-inch microphones, spanning 20 jet diameters with spacing progressing from $0.5D$ to $2.0D$. The conical half-angle of the array is 7 deg. Data are acquired at azimuthal increments of 15 deg over 210 deg of the azimuth.

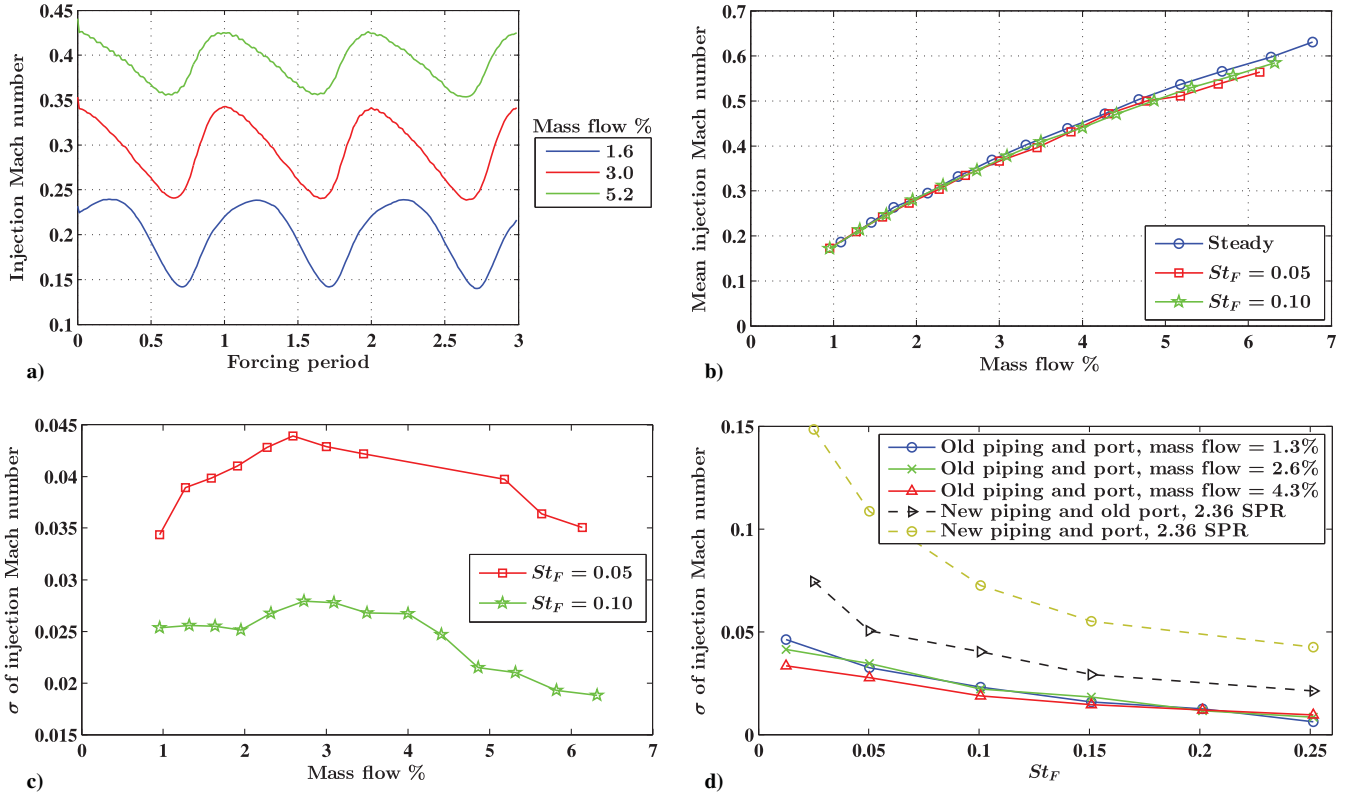

Fig. 3 Original actuator characteristics with phase averaging of injection Mach number: a) waveforms at $St_F = 0.05$ (667 pulses/s); b) steady and c) pulsatile components versus mass flow rate; and d) pulsatile component versus forcing frequency, also showing results with improved piping and injector port design. The standard deviation of the phase-averaged component is denoted σ. The mass flow rate and forcing frequency St_F are referenced to the heated jet operating condition. The SPR is with regard to atmosphere.

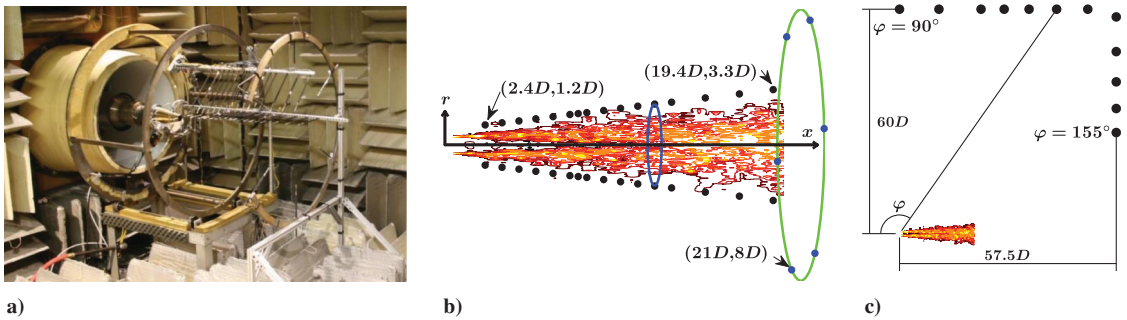

Fig. 4 Setup of microphone arrays: a) rotating near-field pressure array, b) layout of near- and midfield arrays with their (x,r) coordinates, and c) layout of far-field acoustic array.

To center the near-field rotating array on the jet, a laser was mounted parallel to the jet axis using a plug adapter that was attached to the nozzle exit. A pipe was attached to the plug, which extended downstream past the rotating microphone array. The centerline position of the downstream end of the pipe was centered on the laser. The radial locations of the rotating microphones were manually positioned from the pipe reference. The radial locations were verified to be constant at various azimuthal positions of the rotating array, and they were further validated (subsequently) with spectral amplitudes of microphone signals on the fixed array. Sample results are presented in Appendix B.

The far acoustic field was measured at 12 microphone stations, shown schematically in Fig. 4c. The measurements encompassed polar angles from 90 to 155 deg relative to the upstream jet axis at polar radii varying between 60D and 80D. The entire array was in the horizontal plane passing through the jet centerline and containing the two injection ports on either side of it. To facilitate comparison, the far-field sound levels are reported after scaling them to a uniform polar radius of 50D, unless stated otherwise. The quality of the far-field measurements is verified in Appendix B.

In addition, a uniform azimuthal array of six microphones was situated in the intermediate acoustic field at a polar angle of 159 deg and a polar radius of 22.5D (see Fig. 4b). This midfield ring array allowed the resolution of the azimuthal Fourier content of the emitted acoustic (Mach wave) radiation: as a function of the azimuthal structure of the near-field wave packets, on one hand, and the azimuthal forcing pattern, on the other.

All 50 microphones were simultaneously sampled at 200 kHz. Additionally, encoder signals from the two spinning-valve motors were simultaneously recorded for phase-locked postprocessing.

The setup used here permitted significant benefits in terms of diagnosing the downstream evolution and azimuthal structure of near-field wave packets (on the rotating array) and directly connecting them with the evolution and azimuthal structure of the radiated sound (on the ring array). In particular, the Kirchhoff surface methodology mentioned in Sec. I.C allowed us to project, via the wave equation,

the modal amplitudes observed on the near-field array and compare these projections directly with the signals measured on the ring array. In this way, alteration of the near-field wave packets by forcing could be correlated with observed noise reduction, thus providing unambiguous assessment of various hypothesized mechanisms of noise reduction.

F. Survey of Time-Averaged Flowfield

The mean flowfield is the basic ingredient of our wave-packet model of jet noise. The mean flow was measured with a total pressure pitot tube and a total temperature thermocouple with shielding and a bleed vent. The static pressure was obtained using a Pinckney-type probe and used in jet Mach number calculations [49]. The centerline of the jet was sampled at 25 points with logarithmic spacing within $0.25D < x < 30D$. Radial profile surveys were conducted in two azimuthal planes, with the first passing through the center of diametrically opposed injection ports and the second bisecting two ports. Each radial survey consisted of 20 points, which were spaced so as to adequately resolve the developing shear layer.

III. Experimental Results and Analysis

In Secs. III.A and III.B, results are focused on the heated (B122) jet case with axisymmetric steady and unsteady blowing, respectively. Unless noted otherwise, the results presented in these sections are from the final experimental campaign with the improved actuation system, with the injection configured to impinge normal to the primary jet axis. The extensive diagnostic results are analyzed to elucidate the mechanism of noise reduction. In Sec. III.C, we also draw on results from the previous experimental campaigns (with original actuator system) to make comparisons with cold jets, as well as with nonaxisymmetric unsteady forcing and nonnormal impingement. For both steady and unsteady blowing, we report the amplitude of the steady part of the blowing as a percentage mass flow rate referred to the primary jet.

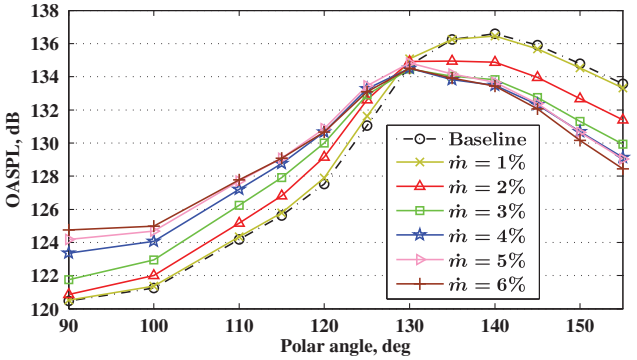

Fig. 5 Overall sound pressure levels versus polar angle for steady blowing with impingement at 90 deg to the jet flow using the improved actuation system. $M_j = 1.5$ and $T_j = 1.74$.

A. Steady Blowing Results

1. *Far-Field Noise Reduction*

Figure 5 reports the overall sound pressure level as a function of polar angle in the heated jet with steady blowing normal to the primary jet axis. We observe significant noise reduction at aft angles near the noise peak, starting at modest mass flow rates, and increasing to about 5 dB at the shallowest angles at a 6% mass flow rate. There is an evident saturation in effectiveness for actuator mass flow rates above 3% that yields at least 3 dB of noise reduction over a range of angles above about 135 deg. At a 150 deg polar angle, a 4 dB OASPL reduction is attained with a 3% mass flow rate at normal impingement. At sideline angles (e.g., 90 deg), where noise amplitude in the natural jet is about 15 dB lower than the peak at 140 deg, steady blowing increases the noise by as much as 5 dB, and there is a crossover from the noise benefit to the penalty at 130 deg. Overall, the forced jet has a broader, less directive, acoustic field than the unforced one.

Figure 6 shows representative spectra at 150 deg (aft) and 90 deg (sideline) polar angles. At aft angles, there is little high-frequency penalty, but some small tones and slight amplification around $St = 1.15$ are evident. This is believed to be associated with noise generated by jet impingement itself. These tones are not self-noise associated with the actuator jets, as the sound pressure level (SPL) in the absence of the primary jet flow (measured separately but not shown here) is about 20 to 30 dB quieter than the tones obtained with both the main and impingement jets operating. The impingement noise is at a frequency that is about 10 times higher as compared to the peak of the aft-angle jet noise at $St \approx 0.1$. This is consistent with the factor-of-10-smaller scale of the actuator nozzle as compared to the primary jet diameter.

At the sideline, where the noise is already some 15 dB quieter than at aft angles, the noise penalty is clearly evident and is seen to increase monotonically with the mass flow rate.

2. *Mean Flow Modifications with Steady Blowing*

Steady blowing changes the mean flowfield of the jet substantially. Defining the end of the potential core as the axial station where the centerline Mach number falls below 99% of the exit velocity, Fig. 7a shows that steady blowing at a 3% mass flow rate reduces the length of the potential core from $6D$ to $4D$. Furthermore, the initial rate of decay of the centerline Mach number is higher as a result of forcing.

Dramatic changes are also observed in the radial profiles at $x = 3D$ in Fig. 7b. In the azimuthal plane of an injection port, the shear layer is squeezed toward the centerline. In between two ports, the shear layer bulges out substantially. Moreover, the shear layer is thickened in both azimuthal planes. To quantify this latter effect, we define the jet momentum thickness Θ at any axial station x and azimuthal angle ϕ as

$$\Theta(x,\phi) = D^{-1}\int_0^{\infty} \frac{\bar{u}_x(x,r,\phi)-u_\infty}{U_j-u_\infty}\left\{1-\frac{\bar{u}_x(x,r,\phi)-u_\infty}{U_j-u_\infty}\right\} r\,\mathrm{d}r \quad (1)$$

where $\bar{u}_x$ is the mean axial velocity, u_∞ is the coflow velocity (associated with the tunnel Mach number M_t), and r is the cylindrical

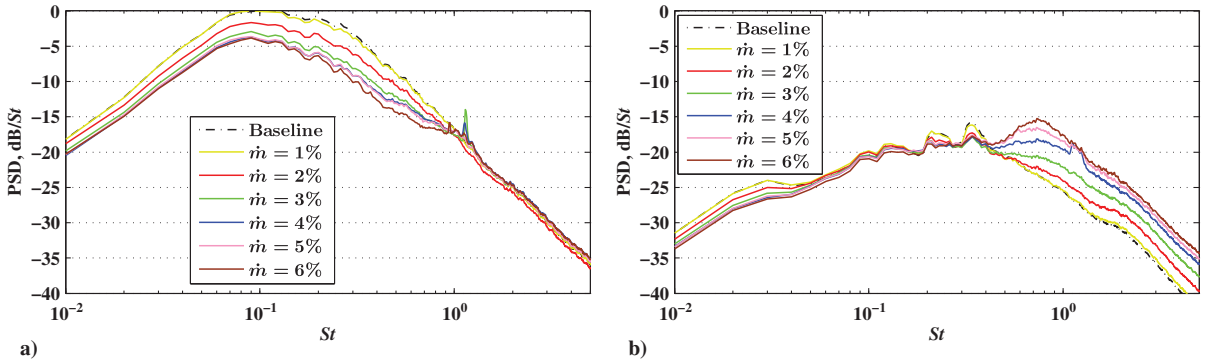

Fig. 6 Far-field sound spectra at a) 150 deg (aft), and b) 90 deg (sideline) polar angle for steady blowing with normal impingement. Spectral levels are relative to baseline peak at 150 deg polar angle. $M_j = 1.5$ and $T_j = 1.74$.

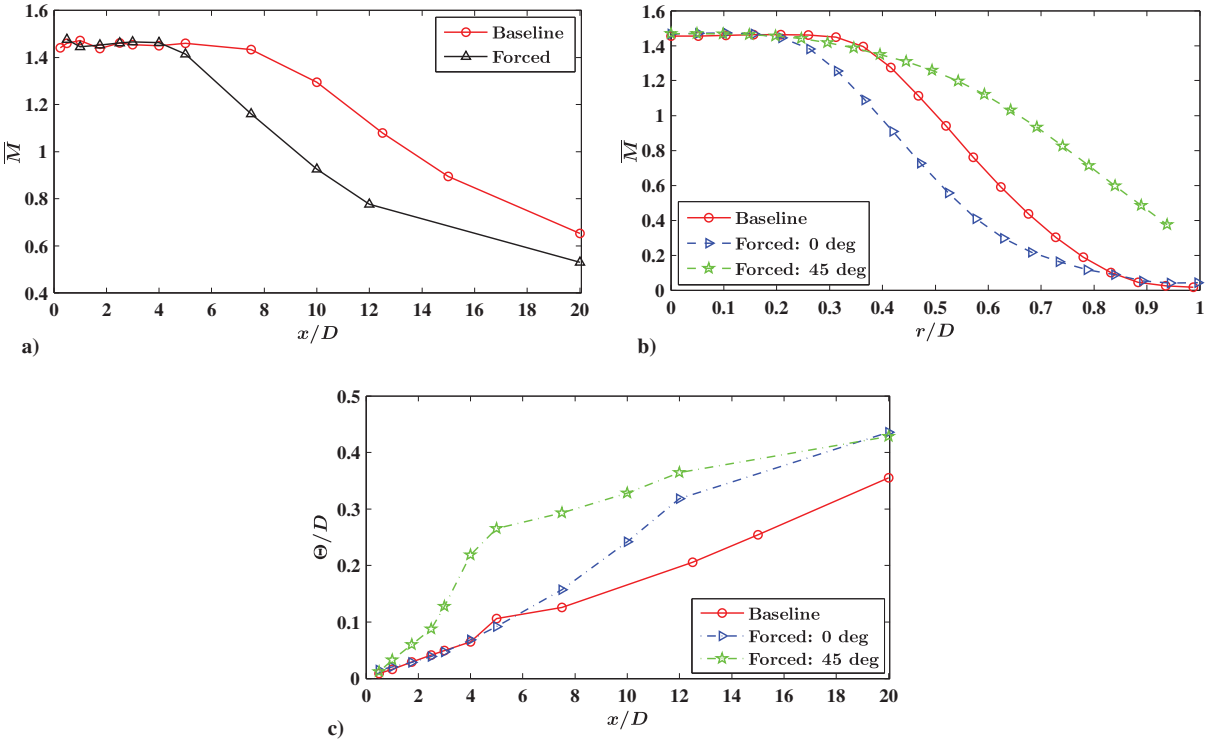

Fig. 7 Effect of steady blowing at 3% mass flow rate with improved actuation system on the mean Mach number a) at the centerline ($r = 0$), b) at $x = 3D$, and c) on the momentum thickness. The azimuthal plane through an injection port is indicated by "0 deg," and "45 deg" implies the plane bisecting two ports. $M_j = 1.5$ and $T_j = 1.74$.

radial coordinate. The momentum thickness is computed at various axial stations in the baseline heated jet, as well as in the forced jet under consideration in the two salient azimuthal planes. The results in Fig. 7c demonstrate the substantial thickening of the shear layer caused by forcing in both azimuthal planes. This thickening persists downstream of the station where the jet becomes approximately circular ($x \geq 20D$).

These modifications to the mean flowfield are similar to those produced by steady microjets [12], wherein the changes are attributed to the development of streamwise vortices similar to those produced by chevrons.

3. *Theoretical Mechanism of Noise Reduction*

The velocity gradient in the shear layer determines the strength of the Kelvin–Helmholtz instability that, in turn, has been shown to account for the growth and evolution of the acoustically dominant wave packets [5]. Thus, the thickening of the shear layer documented in Sec. III.A.2 reduces the growth rate of instabilities, and it is consistent with the lower-amplitude wave-packet activity and reduced noise reported in Sec. III.A.1. In fact, strong evidence exists that corroborates this view that the observed noise reduction is associated with modified wave-packet activity driven by the mean flow changes produced by the jet/actuator interactions rather than, say, by the turbulent structures produced or later excited by those interactions. Figures 8 and 9 present these data, which consist of pressure measurements decomposed into frequency and azimuthal modes on the near-field rotating array and the midfield ring array, respectively.

In Fig. 8, spectral amplitudes and phases (the latter are with reference to the microphone at $x = 5.63D$) for the $m = 0$ and $m = 1$ pressure fluctuations are plotted for several frequencies as a function of downstream position along the conical surface swept by the near-field rotating array. The details of the data processing appear in Appendix A. The amplitude's dimensional units would have been $\mathrm{Pa}/\sqrt{\mathrm{Hz}}$ however, pressure is normalized by $\rho_\infty a_\infty^2$ and frequency is normalized to the Strouhal number. Consistent with our previous studies [5], we interpret these fluctuations as average wave-packet amplitudes. We note that the cross-correlation analysis (not shown here but reported earlier in [48] for a subsonic jet) supports the interpretation in that the pressure fluctuations are highly correlated at all positions along the array depicted in the figure.

Very similar results were presented in [50] for analogous calculations performed on a large-eddy simulation database of the unforced heated jet [34], with the latter having been cross validated against data recorded at the present facility [7]. The calculations in [50] started with an azimuthal Fourier transform of the LES near-field pressure data. On the other hand, the current results were obtained by first computing the azimuthal two-point cross correlations for various azimuthal separations of the microphone arrays, followed by an azimuthal Fourier transform of the cross correlations (see Appendix A). Thus, the results in [50] served to validate the more complicated data-processing methodology pursued here.

Figure 8 compares wave packets in the natural (unforced) jet with those for steady blowing at a 5% mass flow rate using the original actuation system. A reduction in average wave-packet amplitude is observed with steady blowing: most significantly in the $m = 1$ mode. There is also a general trend toward a slower initial growth rate and an ultimately faster decay of the wave packets, which is consistent with the more rapidly spreading mean flowfield. There is no discernible modification in the phase characteristics of the average wave packets.

Thus, the forcing produces average wave packets that are shorter in axial extent and lower in overall amplitude than those in the natural jet. The lowered amplitude is consistent with the greatly reduced aft-angle radiation of the forced jet, whereas the narrowing of the wave-packet envelope is consistent with the broadening of the acoustic field directivity. The latter follows from consideration of the noise radiated by modeled wave packets [5]. Specifically, the narrower envelope in the physical domain results in a broadband distribution of energy with spatial wave number, and thus a more uniform, or less directive, acoustic field.

In Fig. 9, we plot the corresponding pressure amplitudes measured on the midfield ring array. Similar to the data collected on the near-field array, we have processed the data into their spectral components and azimuthal modes. The lines correspond to the measured data and compare the natural and forced jets. Recall that the midfield array is at a polar angle of about 160 deg to the upstream jet axis. Consistent with the far-field noise reduction, we measure significant suppression

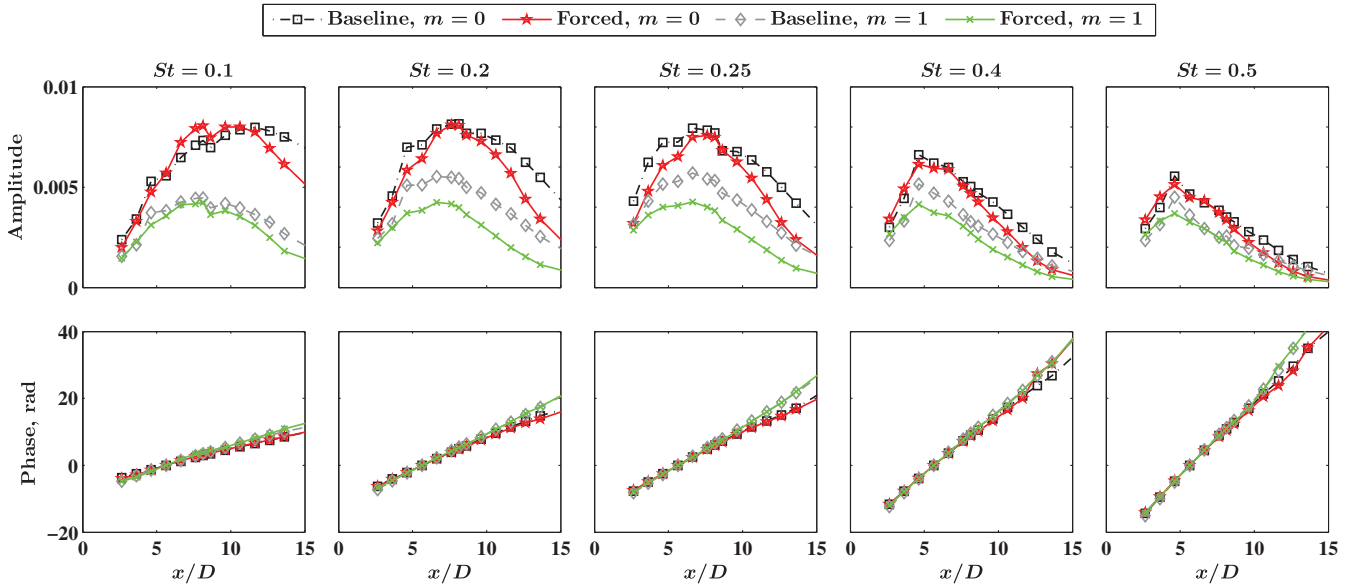

Fig. 8 Near-field pressure amplitude and phase (average wave packets) for the first two azimuthal modes and a range of Strouhal numbers, measured along the rotating cage array for baseline (unforced) jet and with steady blowing at 5% mass flow rate (original actuation system). The phase is with respect to the microphone at $x = 5.63D$. $M_j = 1.5$ and $T_j = 1.74$.

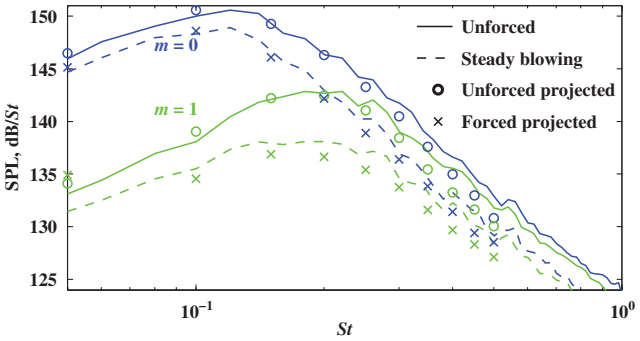

Fig. 9 Pressure amplitude from the midfield azimuthal array corresponding approximately to far-field radiation to an aft angle of 160 deg. Lines are measured spectral amplitudes from the unforced jet (solid) and with steady blowing (dashed) at 5% mass flow rate (original actuation system). Symbols are calculated noise levels based on projection of the average wave-packet evolution measured along the near-field array as shown in Fig. 8. $M_j = 1.5$ and $T_j = 1.74$.

over all frequencies at this far aft angle. At the lowest frequencies, the reduction is greatest for the $m = 1$ mode, but this mode is inefficient at radiating to extreme aft angles: a fact that can be explained by simple noise source models [51]. Over the range of frequencies corresponding to the spectral peak at higher aft angles ($St \sim 0.2$), both $m = 0$ and $m = 1$ are attenuated by a similar amount of about 4 dB/Strouhal number.

As discussed in Sec. I.C, [23] presented a method for predicting the acoustic far field with an equivalent source defined using the two-point space–time correlation of pressure (previously transformed to the temporal and azimuthal Fourier domain) on the conical surface formed by the near-field microphone array surrounding the jet plume. A Gaussian function was fitted to the cross correlation for smooth interpolation on the array. The array was sufficiently far from the noise sources that linear behavior could be assumed, and a Green's function tailored to the conical surface was derived in a Kirchhoff framework for acoustic continuation. The symbols in Fig. 9 show the spectra at the midfield array that have been predicted with this method. The excellent agreement between the measured and inferred noise radiation from each frequency and azimuthal mode directly connects the modified wave-packet activity in the near field with the observed aft-angle noise reduction.

In previous work by Sinha et al., there was success in predicting the wave-packet envelope in the unforced jet based on the PSE representation of the wave packets as instability waves on the turbulent mean flowfield, specifically in the case of chevron jets [35]. We were unable to make the same calculation in the forced jet, owing to the lack of well-resolved mean flow data as well as some technical difficulties in application of linear PSE to forced jets [52]. However, all the aforementioned results support the conclusion that the noise reduction in jets forced with steady blowing (vis-à-vis the natural jet) is caused by changes in the mean turbulent field (produced by actuation). The modified mean flowfield, in turn, provides an altered environment for the streamwise evolution of wave packets that results in a reduction of their associated noise radiation.

We remark that the evidence to date regarding the effect of chevrons on low-frequency aft-angle noise reduction is also consistent with the argued mechanism. In that sense, it is appropriate to think of steady blowing as a kind of fluidic chevron, though, to date, we are unaware of chevron designs for supersonic jets that give rise to the 4–6 dB of aft-angle OASPL noise reduction obtained with steady blowing. Typically, chevron noise reductions are on the order of 2–3 dB at model scale [6,7,53], with engine reductions being smaller at 2 dB [54].

B. Unsteady Blowing Results

We now survey the results obtained with unsteady blowing over a range of frequencies from very low to ones commensurate with the spectral peak. As in the previous section, we concentrate here on results for the heated (B122) jet with all four injector ports actuated in phase simulating the addition of axisymmetric disturbances ($\mu = 0$) to the jet.

1. *Low-Frequency Forcing*

In Sec. I.D, we hypothesized that forcing at very low-frequency forcing ($St \ll 0.1$) could serve as a "phase reference" for naturally occurring wave packets at higher frequencies by reducing variability associated with very slow variations in the effective turbulent mean flowfield in which those wave packets evolved. However, as the actuation system used here produces, at any rotation speed, both a steady and an unsteady component of blowing at each injection port, we must be careful in making comparisons of wave-packet activity with the natural jet. As we have seen in Sec. III.A.2, the steady component of blowing itself gives rise to a substantial change in the turbulent mean flowfield. Ideally, we want to compare wave-packet

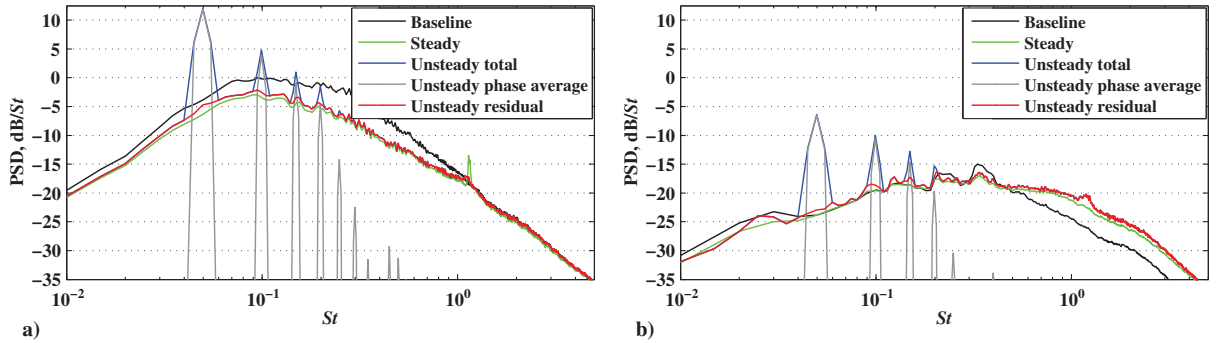

Fig. 10 Comparison in terms of far-field power spectral density (PSD) a) at aft-angle (150 deg) and b) at sideline (90 deg), of the baseline jet and steady and unsteady actuation at $St_F = 0.05$ and $\mu = 0$; both forcing cases are at 3% mass flow rate with the improved actuator. The spectrum for the unsteady forcing case is further divided into the phase-averaged portion (i.e., that part of the acoustic field correlated with actuation) and the uncorrelated residual. All spectra are relative to the baseline jet peak at 150 deg. $M_j = 1.5$ and $T_j = 1.74$.

activity between the unsteadily forced jet and a jet without the unsteady component of forcing but with an equivalent mean flowfield. Thus, we performed a coordinated set of experiments where a given case with unsteady blowing has a paired steady blowing case that has the same mass flow rate (which in turn requires that both conditions use a different supply pressure to the actuation system). Based on earlier mean flow surveys, we believe that this also produces very similar turbulent mean flowfields in both cases.

A set of results for this "variability control" test are given in Fig. 10 for a fixed mass flow rate of 3% using the improved actuation system. For the unsteady actuation, the drum rotation rate is selected to give a pulsation frequency of $St_F = 0.05$ and the azimuthal pattern of forcing is axisymmetric. The SPL results are plotted in the far field at 150 and 90 deg to the upstream jet axis. Comparison of steady and unsteady injections shows that, with the exception of additional tones in the unsteady case, the broadband reductions from the baseline case are identical. From a noise reduction point of view, although the tones themselves may or may not be an additional nuisance, the unsteady blowing is, in this case, counterproductive because it involves a more complicated actuation system and delivers no additional noise benefit when compared to steady actuation with the same level of mass flow rate. We note that similar results, not shown for brevity, were obtained at a lower forcing frequency of $St_F = 0.01$.

In Fig. 10, the pressure data p from the unsteadily forced jets are further decomposed by applying a triple decomposition to the data [55] defined by

$$p = \langle p \rangle + p' = \bar{p} + \tilde{p} + p' \tag{2}$$

where the time average pressure is $\bar{p}$, the phase-averaged portion is $\langle p \rangle$, and the residual is p'. Note that $\tilde{p} = \langle p \rangle - \bar{p}$ is the "coherent" component. We compute $\langle p \rangle$ by averaging each period of data associated with a pulse of the actuators (as recorded by the encoder simultaneously with the microphone data). Specifically, the actuator pulse is subdivided into a number of phases, and all the pressure signal samples that are simultaneous with a particular phase are averaged to arrive at the phase-averaged pressure corresponding to that phase. The $\tilde{p}$ signal is thus, by construction, perfectly correlated with the unsteady actuation; whereas the residual component is perfectly uncorrelated. We interpret the former as noise from the "forced wave packets" and the latter as noise from the "natural" or random wave packets.

We note that, in the general nonlinear case, unsteady forcing can in principle alter both the correlated and random components of the wave packets. However, Fig. 10 shows that the residual component of the unsteadily forced acoustic field is identical to the total acoustic field produced by steady blowing at the equivalent mass flow rate. The strong implication is that the unsteady blowing at low frequency has had no effect on the natural, random evolution of wave packets in the flowfield.

The tonal noise generated by the forced wave packets shows that these structures are excited at much higher amplitudes than exist in the natural baseline jet. At $St_F = 0.05$, we note that the excited wave packets correspond to very long wavelengths. A sequence of harmonics of the forcing frequency are also excited but, as the unsteady forcing is not purely sinusoidal, we believe these harmonics are associated with the actuator waveform rather than nonlinear processes in the wave-packet evolution. Indeed, the near-perfect match between the steady and unsteady forcings with the same mass flow rates yields strong evidence that all the wave packets are evolving in an essentially linear manner on the modified mean turbulent flow associated with the steady part of the blowing.

2. *Higher-Frequency Blowing*

At higher frequencies approaching the peak frequency of wave-packet activity in the natural jet, we expect unsteady actuation to more strongly excite these large-scale structures. One might expect that such strong excitation could lead to nonlinear interactions that might be beneficial for noise reduction. Figure 11 shows results with $St_F = 0.2$ and $\mu = 0$ with mass flow rates of 2 and 3% using the improved actuation system. Each case is compared to steady blowing at the same mass flow rate. These spectra are qualitatively similar to those obtained with lower-frequency actuation (cf. Fig. 10, where St_F is 0.05). In each case, the residual component of the spectrum with unsteady forcing is nearly identical to the case of steady forcing with the same mass flow rate. In this figure, we show that this conclusion extends to data taken along the midfield array, and it is decomposed into azimuthal contributions of modes $m = 0$ and $m = 1$. As we have argued previously, the azimuthally decomposed midfield array data correspond very closely to the near-field wave-packet activity. Thus, these data show that the naturally (randomly) excited wave packets are evolving independently of the directly forced wave packets associated with the (tonal) phase-averaged signal. We note that there is some generation of azimuthal mode $m = 1$ structures correlated to the actuation signal, even though all four actuators are nominally acting in phase ($\mu = 0$). However, the amplitudes of the $m = 1$ tones are small as compared to the corresponding $m = 0$ tones, and they may reflect some small asymmetries in the actuation system.

Regarding the tones, we note that the unsteady component of forcing has increased between the cases with 2 and 3% mass flow rates, and this is evident from the stronger tones emitted in the two cases. However, neither case appears to elicit a nonlinear response of the natural wave packets in the flow.

As in the low-frequency case, this further supports the idea that the natural wave packets are only responding to the time-averaged turbulent flow, which is largely independent of forced structures of higher amplitude that are present in the unsteadily forced jet. From the point of view of noise reduction, it seems that mean flow modifications are the only effective mechanism at the comparative levels of steady and unsteady blowings used in this study. The periodic unsteady component of blowing simply generates periodic wave packets that are not phased to counter the natural occurring random structures. In the absence of wave-packet cancellation, the periodic forced disturbances themselves add tonal noise that is counterproductive to overall noise reduction. In summary, we do not

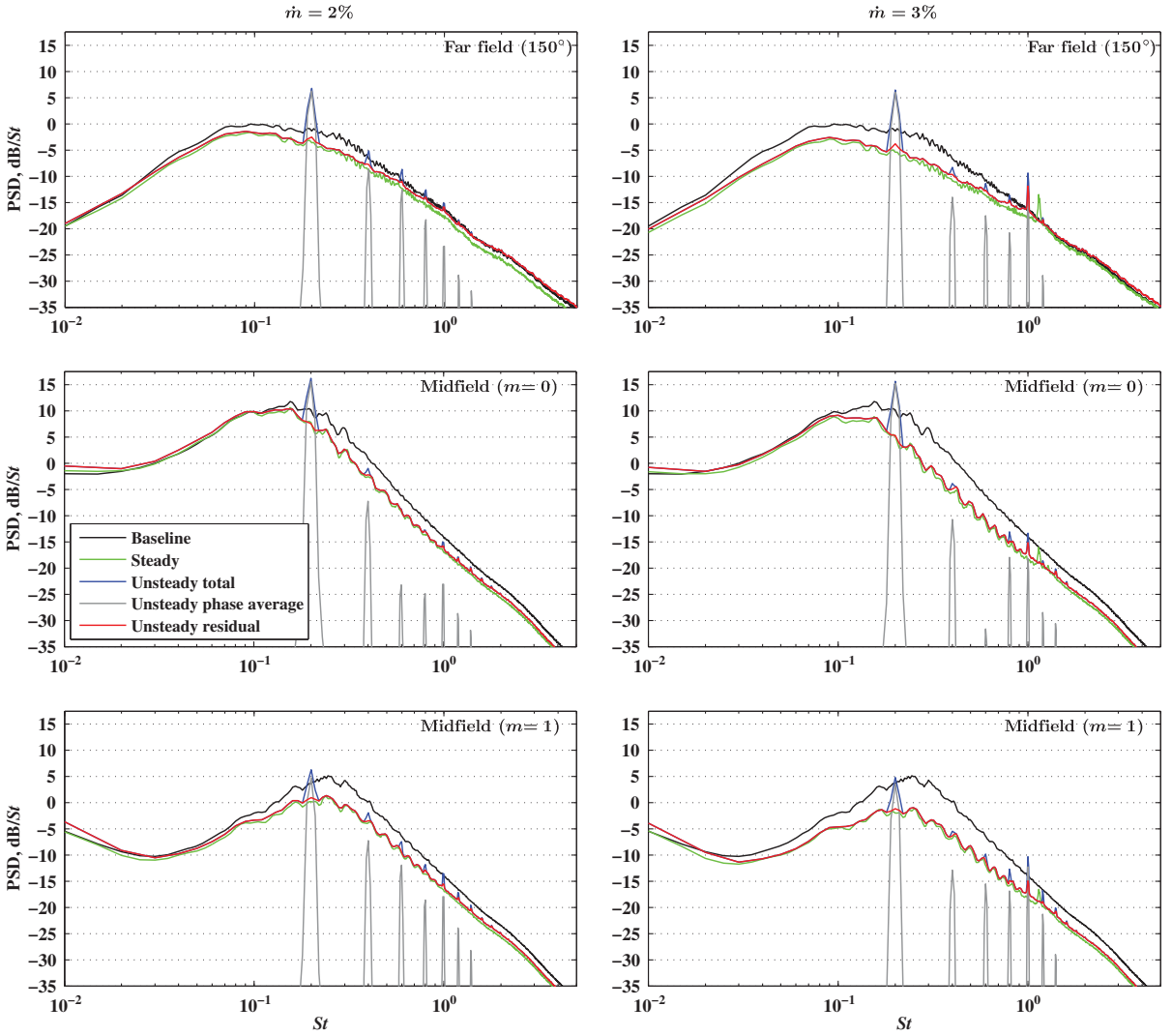

Fig. 11 Comparison of the baseline jet and steady and unsteady actuations at $St_F = 0.2$ and $\mu = 0$ with two different mass flow rates [viz., 2% (left column) and 3% (right column)], using the improved actuation system. Spectra are shown in the far field at a 150 deg polar angle, as well as on the midfield ring array where it is decomposed into azimuthal modes $m = 0$ and $m = 1$. Unsteady spectra are further divided into the phase-averaged and residual portions as in Fig. 10. All spectra are relative to the baseline jet peak at 150 deg in the far field. $M_j = 1.5$ and $T_j = 1.74$.

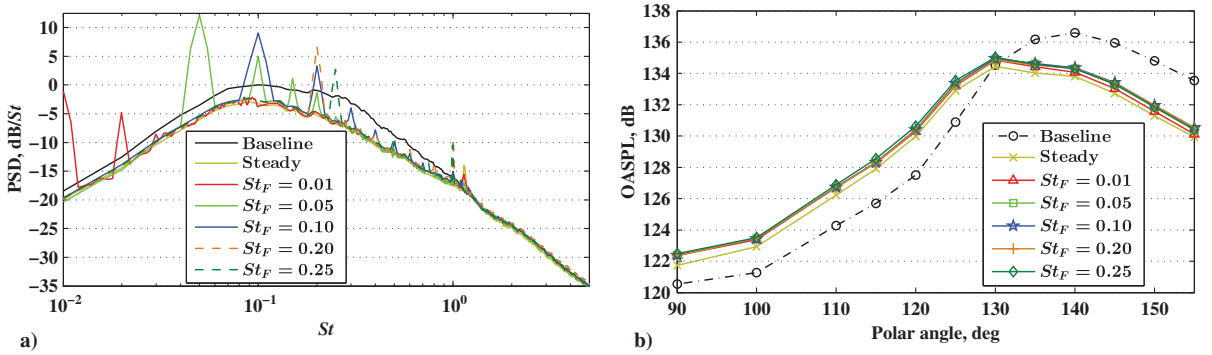

Fig. 12 Far-field acoustic changes due to actuation at various forcing Strouhal numbers (St_F's) in $\mu = 0$ mode with 3% mass flow rate using the improved actuation system. a) Spectra at 150 deg polar angle, normalized to baseline peak. b) Overall sound pressure level of the uncorrelated residual obtained after removing the phase-averaged portion from the microphone signal (for unsteady actuation cases). $M_j = 1.5$ and $T_j = 1.74$.

find support for a nonlinear mechanism in the observed noise reduction.

3. *Survey of Unsteady Actuation Results*

Figure 12 shows the changes in the acoustic far field due to unsteady actuation over a range of St_F at a 3% mass flow rate. As the foregoing discussion has led us to expect, Fig. 12a demonstrates that the broadband spectra at the 150 deg aft angle are independent of the particular St_F, as long as the mean mass flow rate is maintained constant. Specifically, all the unsteady actuation cases along with the corresponding steady blowing case display nearly identical broadband reduction from the baseline SPL. Figure 12b demonstrates

that this behavior of forcing carries over to all the polar angles tested, in terms of the OASPL. To facilitate comparison of the unsteady cases, their OASPLs are calculated from the uncorrelated residuals that remain after subtracting the respective phase-averaged components.

C. Parametric studies

1. *Isothermal Versus Heated Jet*

Holding the jet exit Mach number constant at 1.5, the isothermal and heated jets have different exit velocities that result in acoustic Mach numbers of 1.5 and 1.98, respectively (see Table 1). The primary difference in the radiated sound is associated with progression of the convective Mach number of the turbulent structures from (barely) subsonic in the isothermal case to mildly supersonic in the heated one.

Figure 13 shows contours of the far-field SPL versus polar angle and frequency for both isothermal and heated natural jets. The strong directive nature of the low-frequency sound (toward aft angles) and the more omnidirectional higher-frequency sound are evident in both cases. A shift in the peak angle of radiation occurs as the convection speed of the structures becomes supersonic with respect to ambient in the heated case. For the isothermal jet, the peak directivity occurs at extreme aft angles just beyond the limits of the far-field microphone array. At these very shallow angles to the flow direction, only refraction of sound by the jet's velocity gradient leads to a decreasing sound amplitude in the so-called zone of silence. In the heated jet, the maximum has rotated to a polar angle around 140 deg, which corresponds, by the wavy wall analogy, to structures advecting at $1/\cos(180–140\ \text{deg}) = 1.3$ times the ambient speed of sound or, equivalently, to 65% of the jet exit velocity. This velocity is synonymous with the typical convection speed fraction of 70% measured for turbulent structures. Hence, both pressure and velocity fields are convected at the same speed.

The effect of steady blowing (using the improved actuation system) on the isothermal jet is shown in Figs. 14a and 14b. It should be noted that the primary mass flow rate of the isothermal jet is about 1.3 times that of the heated jet. Thus, a 4.5% injection mass flow rate in the isothermal jet corresponds in the absolute injection rate to a 6% value in the heated jet. With this caveat, we observe that the noise reduction for a given mass injection percentage is more significant in the isothermal jet. In particular, the 3% injection mass flow rate yields a 4.8 dB OASPL reduction at a 155 deg polar angle (where the natural jet's noise peaks). This is obtained with a broadband reduction in SPL, with the maximum being 7.5 dB/Strouhal number at $St = 0.4$. In comparison, with the same mass injection percentage, the heated jet displays 2.7 dB OASPL reduction at its peak polar angle of 140 deg (see Fig. 5), which is obtained with a maximum of 4 dB/Strouhal number broadband SPL reduction at $St = 0.35$ (not shown). If we were to restrict attention to the 155 deg polar angle where the noise reduction peaked in the heated jet also, we would find a 3.7 dB OASPL reduction attended by a maximum of 5.5 dB/Strouhal number broadband SPL reduction.

To compare the effectiveness of steady actuation by holding the absolute injection rate constant, we look at the 4.5 and 6% mass flow cases in the isothermal and heated jets, respectively. With this, the isothermal jet displays a 6 dB OASPL reduction at a 155 deg polar angle, which is attended by a maximum of 9 dB/Strouhal number SPL reduction (at $St = 0.45$). Correspondingly, the heated jet displays a 3.2 dB OASPL reduction at a 140 deg polar angle, with a maximum SPL reduction of 4.5 dB/Strouhal number. Even at the 155 deg polar angle (where the noise reduction peaks), the reduction is 5.2 dB OASPL in the heated jet, which is obtained with a maximum of 7.5 dB/Strouhal number SPL reduction.

Thus, in both methods of comparison, the noise reduction appears to be more significant in the isothermal jet as compared to the heated one. Moreover, in the latter case, the reduction is focused in the direction where the natural jet noise peaks.

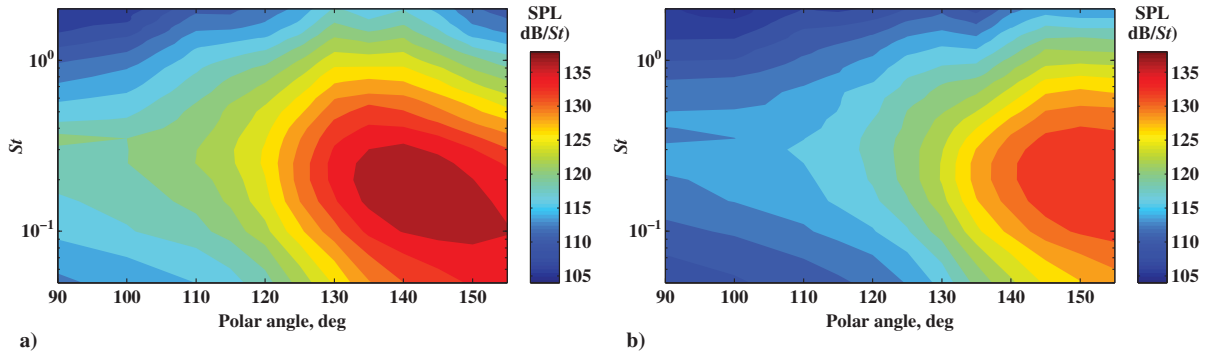

Fig. 13 SPL versus polar angle and frequency for a) heated ($M_j = 1.5$ and $T_j = 1.74$) and b) isothermal ($M_j = 1.5$ and $T_j = 1.0$) natural (unforced) jets.

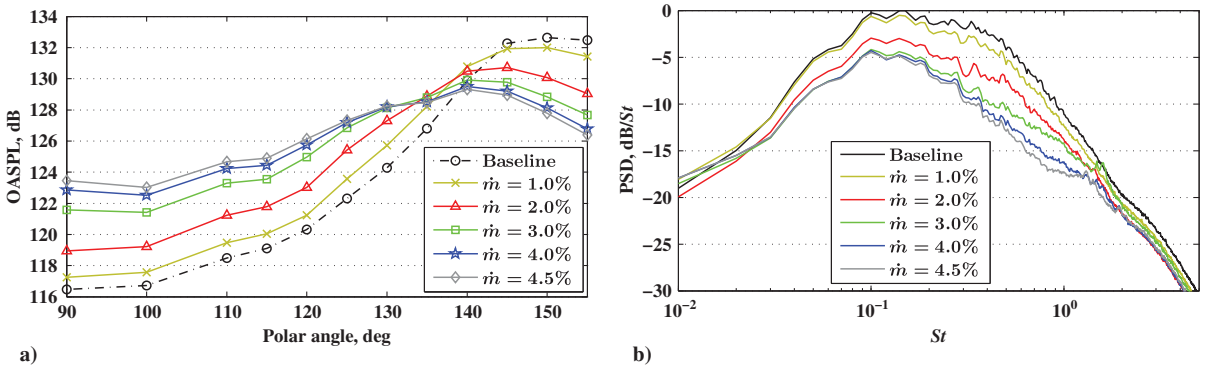

Fig. 14 Acoustics results of steady blowing with normal impingement in $\mu = 0$ mode (using improved actuation system) applied to the isothermal jet ($M_j = 1.5$ and $T_j = 1.0$): a) effect on overall sound pressure level, and b) impact on the spectrum at 155 deg (aft) angle. Spectral levels are relative to baseline peak at 155 deg polar angle.

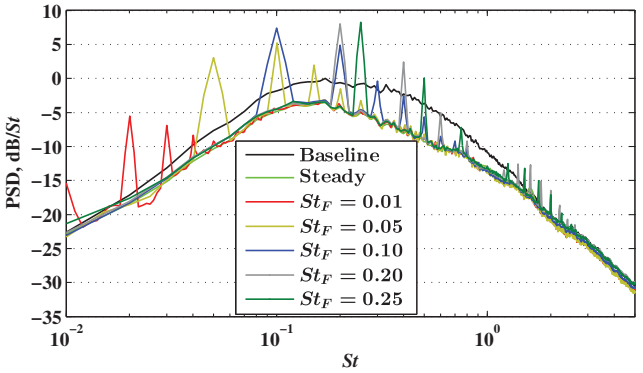

Fig. 15 Impact of various forcing frequencies with 3% mass flow rate in $\mu = 0$ mode (using improved actuation system) on the spectrum at 150 deg polar angle in the isothermal jet ($M_j = 1.5$ and $T_j = 1.0$). All spectral levels are relative to baseline peak at 150 deg polar angle.

It must be remarked from Fig. 14a that the noise penalty at the sideline is commensurately larger for the isothermal jet. In fact, with steady blowing at a 4.5% mass flow rate, the sound field has been rendered substantially omnidirectional. As in the heated jet, the noise mitigation effectiveness in the isothermal jet is seen to be saturating at the upper limit of the injection mass flow rates considered, whereas the attendant noise penalty continues to increase.

In Fig. 15, we explore the effect of unsteady actuation at a 3% mass flow rate on the isothermal jet. As in the case of the heated jet, we find that the unsteady component of forcing is in the linear regime, with the broadband effect being independent of the actuation frequency as long as the mean mass flow rate is held constant.

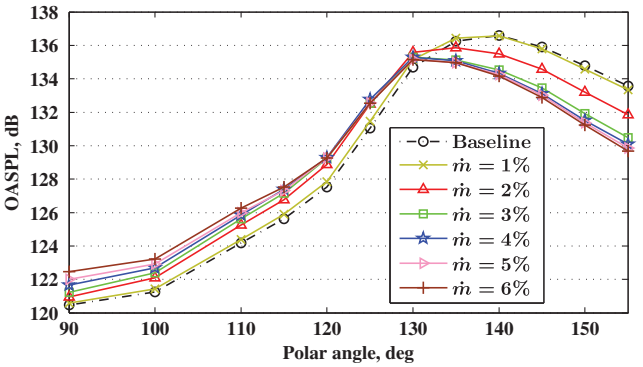

Fig. 16 Overall sound pressure levels versus polar angle for steady blowing with impingement at 30 deg to the jet flow using the improved actuation system. $M_j = 1.5$ and $T_j = 1.74$.

2. *Effect of Injection Angle*

All the preceding results have been obtained with the injection impinging normal to the primary jet axis. The injection angle is known to have an effect on the quantum of noise reduction [56,57]. We evaluated this with our actuator by setting the impingement angle to 30 deg (i.e., the injection is in the approximate primary flow direction and not against it). The OASPL thus obtained is presented as a function of the far-field polar angle for steady blowing on the heated jet in Fig. 16; this should be compared with Fig. 5, which shows the corresponding case of normal impingement. The two results are very similar. However, the 90 deg injection offers somewhat greater reductions, but it also gives rise to a more significant penalty at the sideline, where far-field microphone spectra show that mass injection creates parasitic high-frequency noise (see Fig. 6b). The 30 deg injection angle appears to be a compromise between the aft-angle benefit and the sideline penalty.

3. *Effect of Azimuthal Mode Pattern of Unsteady Actuation*

Finally, we turn our attention to the effect of the azimuthal pattern of unsteady actuation on noise reduction. A limited exploration was made with the available patterns (see Table 2) with the original actuation system on the isothermal jet. Figure 17a compares spectra at 155 deg polar angles for the different patterns. Similar to its invariance to forcing frequency, we find that the broadband spectrum is largely independent of the actuation pattern for a given mass flow rate (which is about 3.9% in this case). We note that the steady offset component of the mass flow rate would be roughly equally distributed among the four injection nozzles; and we would expect, based on the preceding results, the turbulent mean flowfields to be similar in all these cases. The only difference is in the magnitude of tones observed in the acoustic field. Whereas the axisymmetric mode ($\mu = 0$) generates the largest tones, the tonal amplitudes are reduced considerably for the other actuation patterns. Similar observations have been made in jets forced with plasma actuators [15]. This is consistent with the wave-packet models based on instability waves, which show that the axisymmetric mode is more amplified than those occurring at higher azimuthal modes [51]. Clearly, the higher azimuthal modes would be preferable in practices, from the point of view of the tones; but, of course, steady injection is simpler yet and results in about the same broadband noise reduction. This broadband noise reduction is shown in terms of OASPL values in Fig. 17b; these have been obtained after removing the tones using standard spectral processing techniques. Evidently, the effect of different azimuthal patterns of unsteady forcing are indistinguishable in this respect.

IV. Conclusions

Supersonic jet noise reduction was investigated using a spinning-valve actuator that was designed for unsteady air injection near the primary nozzle lip, but which could also act in steady blowing mode. Experiments were conducted on nearly perfectly expanded, supersonic

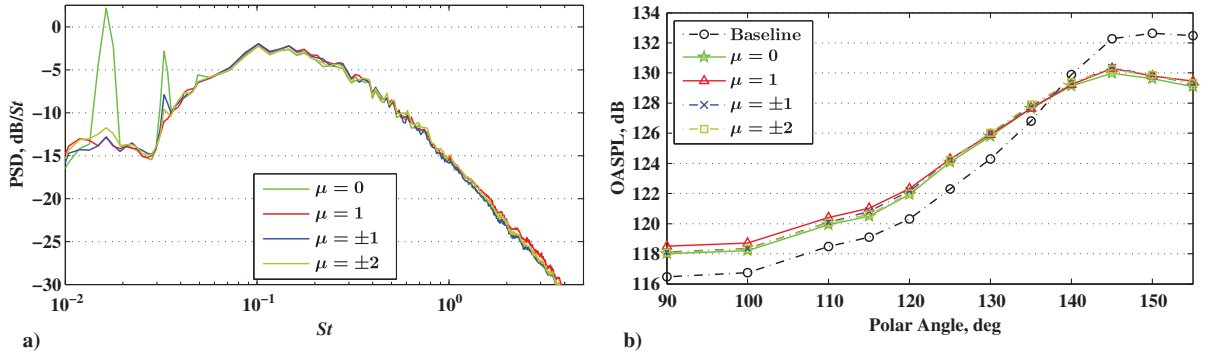

Fig. 17 Effect of azimuthal pattern of unsteady forcing at $St_F = 0.017$ on the far acoustic field: a) SPL at polar angle of 155 deg, and b) OASPL versus polar angle calculated with detoned spectra. The mass flow rate is approximately 3.9% in all cases with the original actuation system. $M_j = 1.5$ and $T_j = 1.0$.

isothermal and heated fully turbulent jets. Focused diagnostics were deployed to investigate the mechanisms of noise mitigation.

Both steady and unsteady blowing resulted in a substantial reduction of the broadband peak aft-angle noise radiation. Reductions of up to 5 dB overall sound pressure level (OASPL) in the peak aft-angle radiation were achieved with steady blowing at an amplitude corresponding to 4% of the mass flow rate of the primary (heated) jet. The noise benefit saturated at mass flow rates above 4%. Increasing the mass flow rate also yielded a monotonically increasing high-frequency noise penalty at the sideline, where baseline noise levels themselves were 15 dB below the aft-angle peak values.

Unsteady blowing with the same mass flow as steady blowing yields similar reductions in broadband OASPL but with additive tones at the forcing frequency and its harmonics. By holding the mass flow rate constant between steady and unsteady blowing cases, it is shown that the noise benefit is uniquely associated with the steady component of blowing.

For steady blowing, the noise reduction appears to occur through an enhancement of the spreading of the turbulent mean flowfield. This mean flowfield is, in turn, consistent with a reduced amplitude of the (stochastic) wave-packet structures: a result that was also directly confirmed by azimuthally decomposing the near- and midfield pressure signals. The modified mean flowfield reduces the growth rate and ultimate amplitude of the wave-packet structures and also narrows their envelope, resulting in a lower-amplitude less directive acoustic field as compared to those associated with the baseline mean flowfield.

The effectiveness of actuation for noise mitigation was more significant in the isothermal jet, with up to a 6 dB OASPL reduction in the peak aft angle, which was attained with steady blowing at a 4.5% mass flow rate. However, this was also accompanied by a greater noise penalty at the sideline angles as compared to the forced heated jet.

The pulsatile component of unsteady blowing generates additional wave packets with amplitudes larger than the naturally occurring stochastic wave packets. The phase-locked wave packets are largely uncorrelated with the natural ones, and thus produce, in an essentially linear way, additional tonal noise. This lack of interaction between the forced and natural wave packets provides further evidence for linear models of wave-packet evolution in supersonic jets. We note that Samimy et al. [15] have shown increased noise mitigation when the jet was forced at combinations of higher Strouhal numbers and azimuthal modes (typically $St > 1$ and $m = 3$) than can be achieved with the spinning-valve actuator. Although this has not been analyzed in their work in the framework of wave packets, similar improvement in noise mitigation effectiveness at higher Strouhal numbers was reported with the rotating centerbody fluidic injection actuator [16] and explained in terms of the linear wave-packet theory, as discussed in Sec. I.B.

The robust linearity of the wave packets has important implications for future efforts aimed at further jet noise reduction. Indeed, rather than developing more aggressive actuators, better outcomes may be expected in the pursuit of feedback control to cancel nascent wave packets. This, in turn, will require development of precursor sensors, diagnostics, and modeling that detects the individual random events that give rise to wave packets. Actuator input will need to be driven by this real-time information through model-based controllers. Progress made in this direction in the setting of the numerical simulation of a planar mixing layer [17] has been discussed in Sec. I.B.

Appendix A: Processing of Near-Field Rotating Microphone Array Data

We outline the processing of the rotating array data required to arrive at the result presented in Fig. 8. Let us denote the pressure measured by a microphone placed at axial coordinate x and azimuthal coordinate ϕ (with regard to the fixed microphone) at time t by $p(x, \phi, t)$; the radial coordinate is redundant, being determined by the conical surface formed by the array. To improve statistical convergence, we divide the entire time series into K (possibly overlapping) segments, with the kth segment being $t \in [t_k^i, t_k^f]$. An estimate of the temporal Fourier coefficient at frequency f is obtained from the kth segment as

$$\check{p}_k(x, \phi; f) := \int_{t_k^i}^{t_k^f} p(x, \phi, t) \mathrm{e}^{-2\pi j f t} \, \mathrm{d}t \tag{A1}$$

where $j = \sqrt{-1}$. In reality, the time series is discretized, and the preceding value must be normalized to render the result independent of the segment length and sampling rate. Moreover, the mean must be subtracted and a windowing function (e.g., Hanning) should be applied before the Fourier transform to avoid spectral leakage at low frequencies.

The two-point cross spectrum of pressure in the frequency domain is estimated as

$$\check{R}_{pp}(x_1, x_2, \phi_1, \phi_2; f) = \frac{1}{K} \sum_{k=1}^{K} \check{p}_k(x_1, \phi_1; f) \check{p}_k^{\dagger}(x_2, \phi_2; f) \tag{A2}$$

where † indicates the complex conjugate. The mth azimuthal Fourier mode of the cross spectrum is found by the usual azimuthal Fourier transform:

$$\hat{R}_{pp}(x_1, x_2; f, m) := \frac{1}{2\pi} \int_0^{2\pi} \check{R}_{pp}(x_1, x_2, \phi_1, \phi_1 + \psi; f) \mathrm{e}^{-jm\psi} \, \mathrm{d}\psi \tag{A3}$$

where ψ is the azimuthal angle difference between two microphones. The amplitude reported in Fig. 8 for a microphone at x_1 is $|\hat{R}_{pp}(x_1, x_1; f, m)|^{1/2}$, and the phase at x_1 with respect to the microphone at x_2 is the angle of the complex quantity $\hat{R}_{pp}(x_1, x_2; f, m)$.

Appendix B: Characteristics of United Technologies Research Center Acoustic Research Tunnel

The acoustic quality of the facility is confirmed in Fig. B1 using the far-field microphone array. Aft angles, where the organized structure noise dominates, show good agreement with earlier studies [58–60].

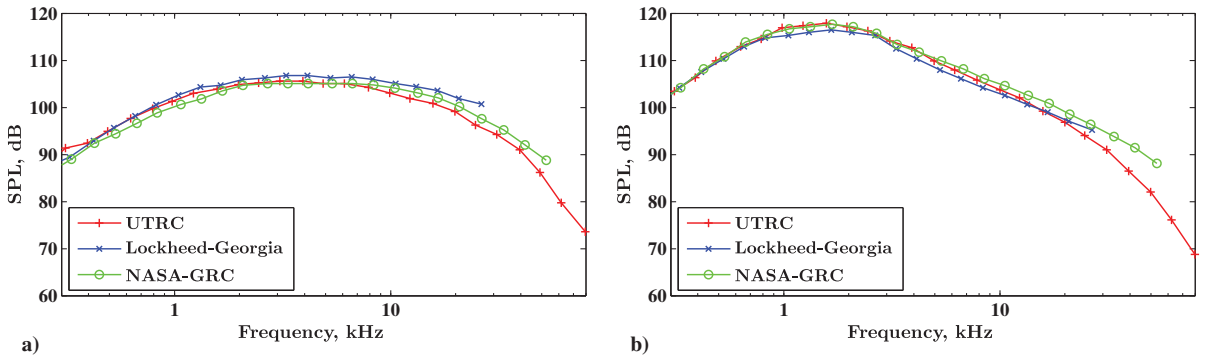

Fig. B1 Far-field acoustic measurements at aft angles of a) 120 deg and b) 150 deg for the $M_j = 1.0$, $T_j = 1.764$ jet as compared with prior studies at Lockheed–Georgia [58,59] and NASA GRC [60]. Figure adopted from [62].

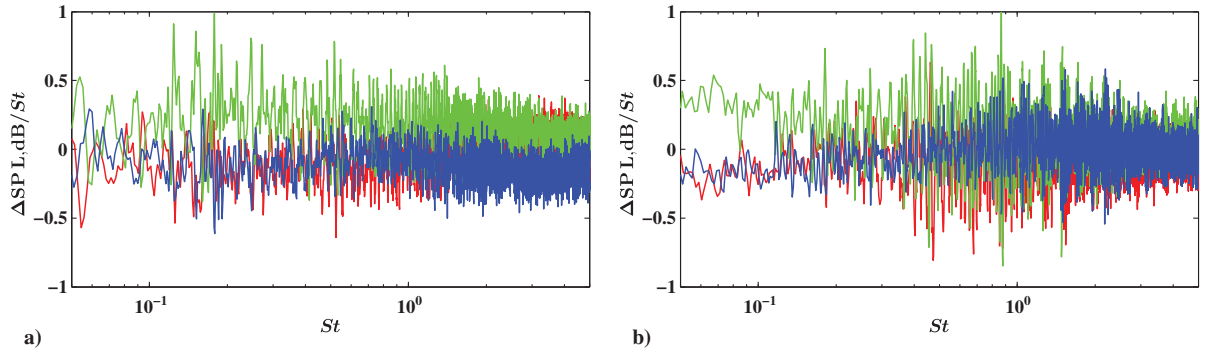

Fig. B2 Repeatability of far-field acoustic measurements at aft angles of a) 120 deg and b) 150 deg, in three separate tests of the unforced $M_j = 1.5$ and $T_j = 1.0$ jet.

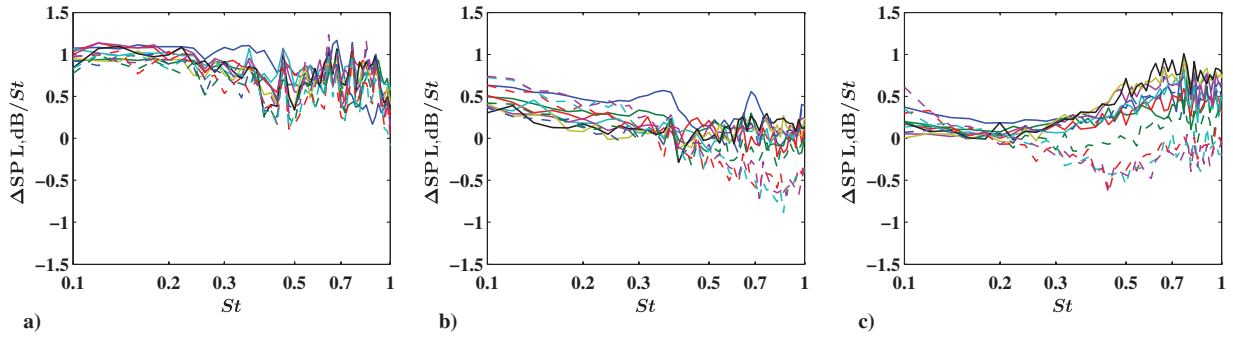

Fig. B3 Concentricity of the near-field rotating microphone array at representative axial stations of a) $x = 5D$, b) $x = 9D$, and c) $x = 16D$, studied with the differences in SPL between corresponding microphones on the rotating and fixed arrays at 12 azimuthal angles of separation between 15 and 180 deg, in the $M_j = 1.5$ and $T_j = 1.0$ jet.

A standard UTRC converging nozzle used for facility calibration was installed in this case. The normalized SPLs were scaled on the Strouhal number and diameter. Atmospheric attenuation was removed (lossless) from the data acquired at the different facility measurement distances and then converted to frequency in Hertz, which was corrected to a common distance of 10 ft, scaled for jet diameter, converted to standard day, rebinned to the UTRC facility analysis bandwidth, and converted from narrowband to third octave. Atmospheric corrections for temperature and humidity effects were based on the approach described in [61].

Repeatability of the experimental data was confirmed by comparing multiple test runs at the same operating conditions. Figure B2 provides narrowband data at the 120 and 150 deg far-field microphones. The data represent the difference between three separate test cases of the isothermal jet. The differences are referenced against the average of the three test cases. The small variance demonstrates good repeatability of the measurements.

The concentricity of the near-field rotating microphone array with the jet axis is essential for accurate estimation of the Fourier azimuthal modes of the hydrodynamic pressure field, and this is studied in Fig. B3. We present the difference in SPL recorded on corresponding microphones of the rotating and fixed arrays for several azimuthal angles of separation in the first two quadrants. At all the three representative axial stations, the variability is within ± 1 dB over the range of Strouhal numbers of interest for wave-packet activity. Noting that the typical hydrodynamic pressure levels are around 150 dB in this region (not shown), the results attest to the high degree of concentricity of the array.

Acknowledgments

The authors gratefully acknowledge support from the Office of Naval Research under contract N0014-11-1-0753 with Joseph Doychak and Brenda Henderson as Technical Monitors and from Naval Air Systems Command under Small Business Technology Transfer contract N68335-11-C-0026 with John Spyropoulos as Technical Monitor.

References

[1] Anderson, T. J., Proscia, T. W., and Cohen, J. M., "Modulation of a Liquid-Fuel Jet in an Unsteady Cross-Flow," *Proceedings of the ASME Turbo Expo*, American Soc. of Mechanical Engineers Paper GT2001-0048, Fairfield, NJ, 2001.

[2] Barooah, P., Anderson, T. J., and Cohen, J. M., "Active Combustion Instability Control with Spinning Valve Actuator," *Journal of Engineering for Gas Turbines and Power*, Vol. 125, No. 4, 2003, pp. 925–932. doi:10.1115/1.1582495

[3] Narayanan, S., Barooah, P., and Cohen, J. M., "Dynamics and Control of an Isolated Jet in Cross Flow," *AIAA Journal*, Vol. 41, No. 12, 2003, pp. 2316–2330. doi:10.2514/2.6847

[4] Tam, C. K. W., "Supersonic Jet Noise," *Annual Review of Fluid Mechanics*, Vol. 27, No. 1, 1995, pp. 17–43. doi:10.1146/annurev.fl.27.010195.000313

[5] Jordan, P., and Colonius, T., "Wave Packets and Turbulent Jet Noise," *Annual Review of Fluid Mechanics*, Vol. 45, No. 1, 2013, pp. 173–195. doi:10.1146/annurev-fluid-011212-140756

[6] Bridges, J. E., and Brown, C. A., "Parametric Testing of Chevrons on Single Flow Hot Jets," *10th AIAA/CEAS Aeroacoustics Conference*, AIAA Paper 2004-2824, 2004.

[7] Schlinker, R. H., Simonich, J. C., Shannon, D. W., Reba, R., Colonius, T., Gudmundsson, K., and Ladiende, F., "Supersonic Jet Noise from Round and Chevron Nozzles: Experimental Studies," *15th AIAA/CEAS Aeroacoustics Conference*, AIAA Paper 2009-3257, 2009.

[8] Seiner, J. M., Ukeiley, L. S., and Jansen, B. J., "Aero-Performance Efficient Noise Reduction for the F404-400 Engine," *11th AIAA/CEAS Aeroacoustics Conference*, AIAA Paper 2005-3048, 2005.

[9] Henderson, B., "Fifty Years of Fluidic Injection for Jet Noise Reduction," *International Journal of Aeroacoustics*, Vol. 9, Nos. 1–2, 2010, pp. 91–122. doi:10.1260/1475-472X.9.1-2.91

[10] Krothapalli, A., Venkatakrshnan, L., Lourenco, L. M., Greska, B., and Elavarasan, R., "Turbulence and Noise Suppression of a High-Speed Jet by Water Injection," *Journal of Fluid Mechanics*, Vol. 491, Sept. 2003, pp. 131–159. doi:10.1017/S0022112003005226

[11] Cuppoletti, D., and Gutmark, E., "Fluidic Injection on a Supersonic Jet at Various Mach Numbers," *AIAA Journal*, Vol. 52, No. 2, 2014, pp. 293–306. doi:10.2514/1.J010000

[12] Alkislar, M. B., Krothapalli, A., and Butler, G. W., "The Effect of Streamwise Vortices on the Aeroacoustics of a Mach 0.9 Jet," *Journal of Fluid Mechanics*, Vol. 578, May 2007, pp. 139–169. doi:10.1017/S0022112007005022

[13] Morris, P. J., McLaughlin, D. K., and Kuo, C.-W., "Noise Reduction in Supersonic Jets by Nozzle Fluidic Inserts," *Journal of Sound and Vibration*, Vol. 332, No. 17, 2013, pp. 3992–4003. doi:10.1016/j.jsv.2012.11.023

[14] Cuppoletti, D., Gutmark, E., Hafsteinsson, H., Eriksson, L.-E., and Prisell, E., "A Comprehensive Investigation of Pulsed Fluidic Injection for Active Control of Supersonic Jet Noise," *51st AIAA Aerospace Sciences Meeting*, AIAA Paper 2013-0009, 2013.

[15] Samimy, M., Kim, J.-H., Kearney-Fischer, M., and Sinha, A., "High-Speed and High Reynolds Number Jet Control Using Localized Arc Filament Plasma Actuators," *Journal of Propulsion and Power*, Vol. 28, No. 2, 2012, pp. 269–280. doi:10.2514/1.B34272

[16] Kœnig, M., Sasaki, K., Cavalieri, A. V. G., Jordan, P., and Gervais, Y., "Jet-Noise Control by Fluidic Injection from a Rotating Plug: Linear and Nonlinear Sound-Source Mechanisms," *Journal of Fluid Mechanics*, Vol. 788, Feb. 2016, pp. 358–380. doi:10.1017/jfm.2015.670

[17] Sasaki, K., Tissot, G., Cavalieri, A. V. G., Silvestre, F. J., Jordan, P., and Biau, D., "Closed-Loop Control of Wavepackets in a Free Shear-Flow," *22nd AIAA/CEAS Aeroacoustics Conference*, AIAA Paper 2016-2758, 2016.

[18] Mollo-Christensen, E., "Jet Noise and Shear Flow Instability Seen from an Experimenter's Point of View," *Journal of Applied Mechanics*, Vol. 34, No. 1, 1967, pp. 1–7. doi:10.1115/1.3607624

[19] Liu, J. T. C., "Developing Large-Scale Wavelike Eddies and the Near Jet Noise Field," *Journal of Fluid Mechanics*, Vol. 62, No. 3, 1974, pp. 437–464. doi:10.1017/S0022112074000772

[20] Arndt, R. E. A., Long, D. F., and Glauser, M. N., "The Proper Orthogonal Decomposition of Pressure Fluctuations Surrounding a Turbulent Jet," *Journal of Fluid Mechanics*, Vol. 340, No. 1, 1997, pp. 1–33. doi:10.1017/S0022112097005089

[21] Jordan, P., Coiffet, F., Delville, J., Gervais, Y., and Ricaud, F., "Acoustic-Hydrodynamic Interaction in the Entrainment Region of Subsonic Jet Flow," *10th AIAA/CEAS Aeroacoustics Conference*, AIAA Paper 2004-3020, 2004.

[22] Suzuki, T., and Colonius, T., "Instability Waves in a Subsonic Round Jet Detected Using a Near-Field Phased Microphone Array," *Journal of Fluid Mechanics*, Vol. 565, Oct. 2006, pp. 197–226. doi:10.1017/S0022112006001613

[23] Reba, R., Narayanan, S., and Colonius, T., "Wave-Packet Models for Large-Scale Mixing Noise," *International Journal of Aeroacoustics*, Vol. 9, Nos. 4–5, 2010, pp. 533–557. doi:10.1260/1475-472X.9.4-5.533

[24] Michalke, A., and Fuchs, H. V., "On Turbulence and Noise of an Axisymmetric Shear Flow," *Journal of Fluid Mechanics*, Vol. 70, No. 1, 1975, pp. 179–205. doi:10.1017/S0022112075001966

[25] Crighton, D. G., and Gaster, M., "Stability of Slowly Diverging Jet Flow," *Journal of Fluid Mechanics*, Vol. 77, No. 2, 1976, pp. 397–413. doi:10.1017/S0022112076002176

[26] Zaman, K. B. M. Q., and Hussain, A. K. M. F., "Vortex Pairing in a Circular Jet Under Controlled Excitation. Part 1. General Jet Response," *Journal of Fluid Mechanics*, Vol. 101, No. 3, 1980, pp. 449–491. doi:10.1017/S0022112080001760

[27] Mankbadi, R., and Liu, J. T. C., "A Study of the Interactions Between Large-Scale Coherent Structures and Fine-Grained Turbulence in a Round Jet," *Proceedings of the Royal Society of London, Series A: Mathematical and Physical Sciences*, Vol. 298, No. 1443, 1981, pp. 541–602.

[28] Tam, C. K. W., and Morris, P. J., "The Radiation of Sound by the Instability Waves of a Compressible Plane Turbulent Shear Layer," *Journal of Fluid Mechanics*, Vol. 98, No. 2, 1980, pp. 349–381. doi:10.1017/S0022112080000195

[29] Tam, C. K. W., and Morris, P. J., "Tone Excited Jets, Part V: A Theoretical Model and Comparison with Experiment," *Journal of Sound and Vibration*, Vol. 102, No. 1, 1985, pp. 119–151. doi:10.1016/S0022-460X(85)80106-1

[30] Brown, C. A., and Bridges, J. E., "Acoustic Efficiency of Azimuthal Modes in Jet Noise Using Chevron Nozzles," NASA TM-2006-214364, 2006.

[31] Gudmundsson, K., and Colonius, T., "Instability Wave Models for the Near-Field Fluctuations of Turbulent Jets," *Journal of Fluid Mechanics*, Vol. 689, Dec. 2011, pp. 97–128. doi:10.1017/jfm.2011.401

[32] Cavalieri, A. V. G., Rodríguez, D., Jordan, P., Colonius, T., and Gervais, Y., "Wavepackets in the Velocity Field of Turbulent Jets," *Journal of Fluid Mechanics*, Vol. 730, Sept. 2013, pp. 559–592. doi:10.1017/jfm.2013.346

[33] Sinha, A., Rodríguez, D., Brès, G., and Colonius, T., "Wavepacket Models for Supersonic Jet Noise," *Journal of Fluid Mechanics*, Vol. 742, 2014, pp. 71–95. doi:10.1017/jfm.2013.660

[34] Brès, G. A., Ham, F. E., Nichols, J. W., and Lele, S. K., "Unstructured Large-Eddy Simulations of Supersonic Jets," *AIAA Journal*, Vol. 55, No. 4, 2017, pp. 1164–1184. doi:10.2514/1.J055084

[35] Sinha, A., Gudmundsson, K., Xia, H., and Colonius, T., "Parabolized Stability Analysis of Jets from Serrated Nozzles," *Journal of Fluid Mechanics*, Vol. 789, 2016, pp. 36–63. doi:10.1017/jfm.2015.719

[36] Cavalieri, A. V. G., Jordan, P., Agarwal, A., and Gervais, Y., "Jittering Wave-Packet Models for Subsonic Jet Noise," *Journal of Sound and Vibration*, Vol. 330, Nos. 18–19, 2011, pp. 4474–4492. doi:10.1016/j.jsv.2011.04.007

[37] Kerhervé, F., Cordier, L., and Jordan, P., "A Twenty Degree-of-Freedom Model of Sound Source Dynamics in a Turbulent Jet," *18th AIAA/CEAS Aeroacoustics Conference*, AIAA Paper 2012-2255, 2012.

[38] Jordan, P., Colonius, T., Brès, G. A., Zhang, M., Towne, A., and Lele, S.., "Modeling Intermittent Wavepackets and Their Radiated Sound in a Turbulent Jet," *Proceedings of the Summer Program*, Center for Turbulence Research, Stanford Univ., 2014, p. 241.

[39] Baqui, Y. B., Agarwal, A., Cavalieri, A. V. G., and Sinayoko, S., "A Coherence-Matched Linear Source Mechanism for Subsonic Jet Noise," *Journal of Fluid Mechanics*, Vol. 776, 2015, pp. 235–267. doi:10.1017/jfm.2015.322

[40] Wei, M., and Freund, J. B., "A Noise-Controlled Free Shear Flow," *Journal of Fluid Mechanics*, Vol. 546, 2006, pp. 123–152. doi:10.1017/S0022112005007093

[41] Kim, J., Bodony, D. J., and Freund, J. B., "Adjoint-Based Control of Loud Events in a Turbulent Jet," *Journal of Fluid Mechanics*, Vol. 741, 2014, pp. 28–59. doi:10.1017/jfm.2013.654

[42] Paterson, R. W., Vogt, P. G., and Foley, W. M., "Design and Development of the United Aircraft Research Laboratories Acoustic Research Tunnel," *Journal of Aircraft*, Vol. 10, No. 7, 1973, pp. 427–433. doi:10.2514/3.60243

[43] Simonich, J. C., Narayanan, S., and Schlinker, R. H., "Facility and Data Quality Issues for Scale-Model Jet Noise Testing," *41st AIAA Aerospace Sciences Meeting and Exhibit*, AIAA Paper 2003-1057, 2003.

[44] Tanna, H. K., "An Experimental Study of Jet Noise. Part I: Turbulent Mixing Noise," *Journal of Sound and Vibration*, Vol. 50, No. 3, 1977, pp. 405–428. doi:10.1016/0022-460X(77)90493-X

[45] Schlinker, R. H., Simonich, J. C., and Reba, R., "Simulated Flight Effects on Supersonic Jet Noise from Round Nozzles," *16th AIAA/CEAS Aeroacoustics Conference*, AIAA Paper 2010-3925, 2010.

[46] Bruun, H. H., *Hot-Wire Anemometry: Principles and Signal Analysis*, Oxford Univ. Press, New York, 1995, pp. 214–218.

[47] Kim, B.-H., Williams, D. R., Emo, S., and Acharya, M., "Modeling Pulsed-Blowing Systems for Flow Control," *AIAA Journal*, Vol. 43, No. 2, 2005, pp. 314–325. doi:10.2514/1.10285

[48] Reba, R., Simonich, J. C., and Schlinker, R. H., "Measurement of Source Wave-Packets in High-Speed Jets and Connection to Far-Field Sound," *14th AIAA/CEAS Aeroacoustics Conference*, AIAA Paper 2008-2891, 2008.

[49] Pinckney, S. Z., "A Short Static-Pressure Probe Design for Supersonic Flow," NASA TN D-7978, 1975.

[50] Rodríguez, D., Sinha, A., Brès, G., and Colonius, T., "Inlet Conditions for Wave Packet Models in Turbulent Jets Based on Eigenmode

Decomposition of Large Eddy Simulation Data," *Physics of Fluids*, Vol. 25, 2013, Paper 105107.

[51] Cavalieri, A. V. G., Jordan, P., Colonius, T., and Gervais, Y., "Axisymmetric Superdirectivity in Subsonic Jets," *Journal of Fluid Mechanics*, Vol. 704, 2012, pp. 388–420. doi:10.1017/jfm.2012.247

[52] Sinha, A., Schlinker, R. H., Simonich, J. C., Reba, R., and Colonius, T., "Toward Active Control of Noise from Hot Supersonic Jets," *19th AIAA/CEAS Aeroacoustics Conference*, AIAA Paper 2013-2234, 2013.

[53] Callender, B., Gutmark, E. J., and Martens, S., "Far-Field Acoustic Investigation into Chevron Nozzle Mechanisms and Trends," *AIAA Journal*, Vol. 43, No. 1, 2005, pp. 87–95. doi:10.2514/1.6150

[54] Martens, S., and Spyropoulos, J. T., "Practical Jet Noise Reduction for Tactical Aircraft," *Proceedings of the ASME Turbo Expo*, American Soc. of Mechanical Engineers Paper GT2010-23699, Fairfield, NJ, 2010.

[55] Hussain, A. K. M. F., and Reynolds, W. C., "The Mechanics of an Organized Wave in Turbulent Shear Flow," *Journal of Fluid Mechanics*, Vol. 41, No. 2, 1970, pp. 241–258. doi:10.1017/S0022112070000605

[56] Norum, T. D., "Reductions in Multi-Component Jet Noise by Water Injection," *10th AIAA/CEAS Aeroacoustics Conference*, AIAA Paper 2004-2976, 2004.

[57] Greska, B., "Supersonic Jet Noise and Its Reduction Using Microjet Injection," Ph.D. Thesis, Dept. of Mechanical Engineering, Florida State Univ., Tallahassee, FL, 2005.

[58] Tanna, H. K., Dean, P. D., and Burrin, R. H., "The Influence of Temperature on Shock-Free Supersonic Jet Noise," *Journal of Sound and Vibration*, Vol. 39, No. 4, 1975, pp. 429–460. doi:10.1016/S0022-460X(75)80026-5

[59] Tanna, H. K., Dean, P. D., and Burrin, R. H., "The Generation and Radiation of Supersonic Jet Noise. Volume 3. Turbulent Mixing Noise Data," U.S. Air Force Aero Propulsion Lab. TR-76-65, 1976.

[60] Brown, C. A., and Bridges, J. E., "Small Hot Jet Acoustic Rig Validation," NASA TM-2006-214234, 2006.

[61] Bass, H. E., Sutherland, L. C., Zuckerwar, A. J., Blackstock, D. T., and Hester, D. M., "Atmospheric Absorption of Sound: Further Developments," *Journal of the Acoustical Society of America*, Vol. 97, No. 1, 1995, pp. 680–683; also, Erratum, *Journal of the Acoustical Society of America*, Vol. 99, No. 2, 1996, p. 1259. doi:10.1121/1.412989

[62] Schlinker, R. H., Simonich, J. C., Reba, R., Colonius, T., and Ladiende, F., "Decomposition of High Speed Jet Noise: Source Characteristics and Propagation Effects," *14th AIAA/CEAS Aeroacoustics Conference*, AIAA Paper 2008-2890, 2008.

L. Ukeiley
Associate Editor